Received: 28 November 2022 | Revised: 20 February 2023 | Accepted: 26 February 2023

DOI: 10.1002/gea.21959

RESEARCH ARTICLE

Geoarchaeology An International Journal WILEY

Lidar visualization techniques for the construction of geoarchaeological deposit models: An overview and evaluation in alluvial environments

Nicholas Crabb[1] | Chris Carey[1] | Andy J. Howard[2] | Matthew Brolly[1]

[1]University of Brighton, Brighton, UK

[2]Landscape and Research Management, Bridgnorth, Stanmore, UK

Correspondence
Nicholas Crabb, Centre for Earth Observation Science, University of Brighton, Lewes Rd, Brighton, UK.
Email: n.crabb@brighton.ac.uk

Scientific editing by Edward Henry.

Funding information
UK Research and Innovation

Abstract

Lidar has become an essential tool for the mapping and interpretation of natural and archaeological features within the landscape. It is also increasingly integrated and visualized within geoarchaeological deposit models, providing valuable topographic and stratigraphic control from the contemporary ground surface downwards. However, there is a wide range of methods available for the visualization of lidar elevation models and a review of existing research suggests that it remains unclear which are most appropriate for geoarchaeological applications. This paper addresses this issue by providing an overview and quantitative evaluation of these techniques with examples from archaeologically resource-rich alluvial environments. Owing to the relatively low-relief nature of the terrain within these temperate lowland flood plain environments, the results show that there is a small number of visualization methods that demonstrably improve the detection of geomorphological landforms that can be related to the variable distribution of archaeological resources. More specifically, a combination of Relative Elevation Models combined with Simple Local Relief Models offered an optimal approach that subsequently allows integration with deposit models. Whilst the presented examples are from a flood plain setting, deposit models are pertinent to a range of landscape contexts and the methodology applied here has wider applicability.

KEYWORDS
alluvial environments, geoarchaeological deposit modelling, lidar visualization, remote sensing, separability analysis

1 | INTRODUCTION

Geoarchaeological deposit models are exceptionally useful tools for investigating the archaeological record and associated landscape evolution. They provide a framework for understanding subsurface sediment architectures, processes and depositional environments, which in turn can be used to inform strategies for geoprospection (e.g., the identification of culturally rich sediment units and their spatial distribution). This typically comprises a visual representation of spatial and stratigraphic relationships between natural subsurface sediments, palaeoenvironmental remains and archaeological features (Carey et al., 2018; Historic England, 2020). However, deposit models vary

significantly in terms of their visual outputs from relatively simple two-dimensional vertical cross-sections and horizontal surfaces to more computationally demanding deposit thickness maps and pseudo-three-dimensional models. Some advanced deposit models also integrate a range of airborne and terrestrial remote sensing (Carey et al., 2019; Crabb et al., 2022; Schmidt et al., 2019) and geophysical survey data (Bates & Bates, 2016; Engel et al., 2022; Verhegge et al., 2016, 2021). Yet, the coalescing of such disparate, albeit complementary, measurements of flood plain surface features together with records of subsurface sediment stratigraphy and architecture is not straightforward. In particular, lidar data have become a vital part of developing very accurate three-dimensional (3D) models, but it is questionable whether these data are used to their full potential within geoarchaeological investigations. Consequently, this paper aims to explore this potential, review how lidar has been previously applied and establish several key parameters for its future inclusion within geoarchaeological projects.

1.1 | Deposit modelling in archaeology

Although the specific term 'deposit model' is not always applied, in the last decade, there has been an increasing number of geoarchaeological investigations that produced land classifications to construct a 'model' of the subsurface. Such an approach is widely used across Europe and North America, either to inform research-driven projects (e.g., Bini et al., 2015; Carlson & Baichtal, 2015; Castanet et al., 2022; van Dinter et al., 2017; Fontana et al., 2017; Gregory et al., 2021; Mozzi et al., 2018) or as part of the design of mitigation and heritage management strategies within commercial archaeology (Carey et al., 2019; Gearey et al., 2016; Stastney et al., 2021). Most of the models produced by such investigations are managed and generated using computational and GIS tools, but there is also a range of software available that has enabled more widespread construction of deposit models in recent years (e.g., Rockworks, Groundhog, Voxler, Strater, etc.). In tandem with this, several 'best practice' papers have recently been drafted to provide guidance for their wider application by practitioners, consultants and planning archaeologists (Carey et al., 2019; Historic England, 2020). Whilst these documents allude to the incorporation of lidar and other remote sensing data sets for the definition of surface topography and landforms, there is limited discussion as to how best to achieve this. Moreover, most applications of lidar data within geoarchaeological deposit modelling contexts utilize relatively simple or unaltered visualizations of lidar-derived Digital Elevation Models (DEM). However, a better definition of features may be achieved through additional visual enhancements, but there has been little discussion/research into which techniques are most appropriate.

A focused search of existing English-language literature containing the keywords 'Lidar' and 'Geoarchaeology' using Google Scholar and Scopus (Elsevier's abstract and citation database) in September 2022 returned 71 items dating from 2006. These principally comprise research articles as well as a small number of book sections and conference proceedings concerned with regions in the temperate zone (Figure 1). Of these, 72% dealt with alluvial environments, and around half include an interpretation analogous to a deposit model (i.e., they map the distribution of buried deposits of geoarchaeological interest across a site or landscape). In each case, lidar is integrated into the analysis to some extent, but only 18% use additional data transformation techniques to enhance the visibility of resources. In addition, there is frequently little or no justification for the selection of these visualizations, although there are exceptions to this (Mayoral et al., 2017). For example, hillshading is very widely used, but there is rarely an explanation as to what advantage this has over other visualization techniques or unaltered versions of lidar DEM. While alternative visualizations may not always be appropriate or necessary for every project, they have the potential to define a wide range of features and landforms more accurately. As such, this paper aims to provide a detailed review and case study of the suitability and efficacy of visualization techniques applied for the identification of geoarchaeological resources within the valley floors of the rivers Lugg and Wye, Herefordshire (UK). It is hoped that this study will facilitate wider integration of appropriate visualizations of lidar-derived DEMs into investigations of complex depositional environments not only within fluvial systems but also more broadly within the study of sediment systems.

1.2 | Using lidar to define the archaeological potential

Within many parts of the temperate zone, postglacial lowland flood plains are low- relief environments containing a complex assemblage of alluvial landforms that provide a record of the evolution of the river system (Brown, 1997; Howard et al., 2015). Topographic expressions of natural landforms such as palaeochannels, gravel islands, levees, bars and other bedforms may be present and can exert a significant influence on past settlement patterns, human exploitation and impact on the landscape (Carey et al., 2017). Mapping and understanding these landform assemblages can, therefore, offer significant insights into the distribution of archaeological remains (Carey et al., 2006; Challis & Howard, 2003, 2006; Passmore & Waddington, 2009). However, the lateral and vertical accretion of fine-grained alluvial sediments within lowland flood plains, which are associated with human activity and land-use changes, can conceal and/or reduce the topographic expressions of these landforms (Brown, 2009; French, 2003; Howard & Macklin, 1999). Thus, while lidar visualizations aid in the interpretation of geomorphological processes and landscape evolution, they cannot be taken at face value and are most effective when integrated with other intrusive data sets (e.g., boreholes, test-pitting, etc.) or deeper methods of geophysical survey such as low-frequency ground penetrating radar (GPR), electrical resitivity tomography (ERT), or electromagnetic induction (EM) (Bates & Bates, 2016; Engel et al., 2022; Verhegge et al., 2016, 2021).

Over the last two decades, lidar has become a staple method used within both landscape archaeological and geoarchaeological projects, primarily within temperate regions of the northern

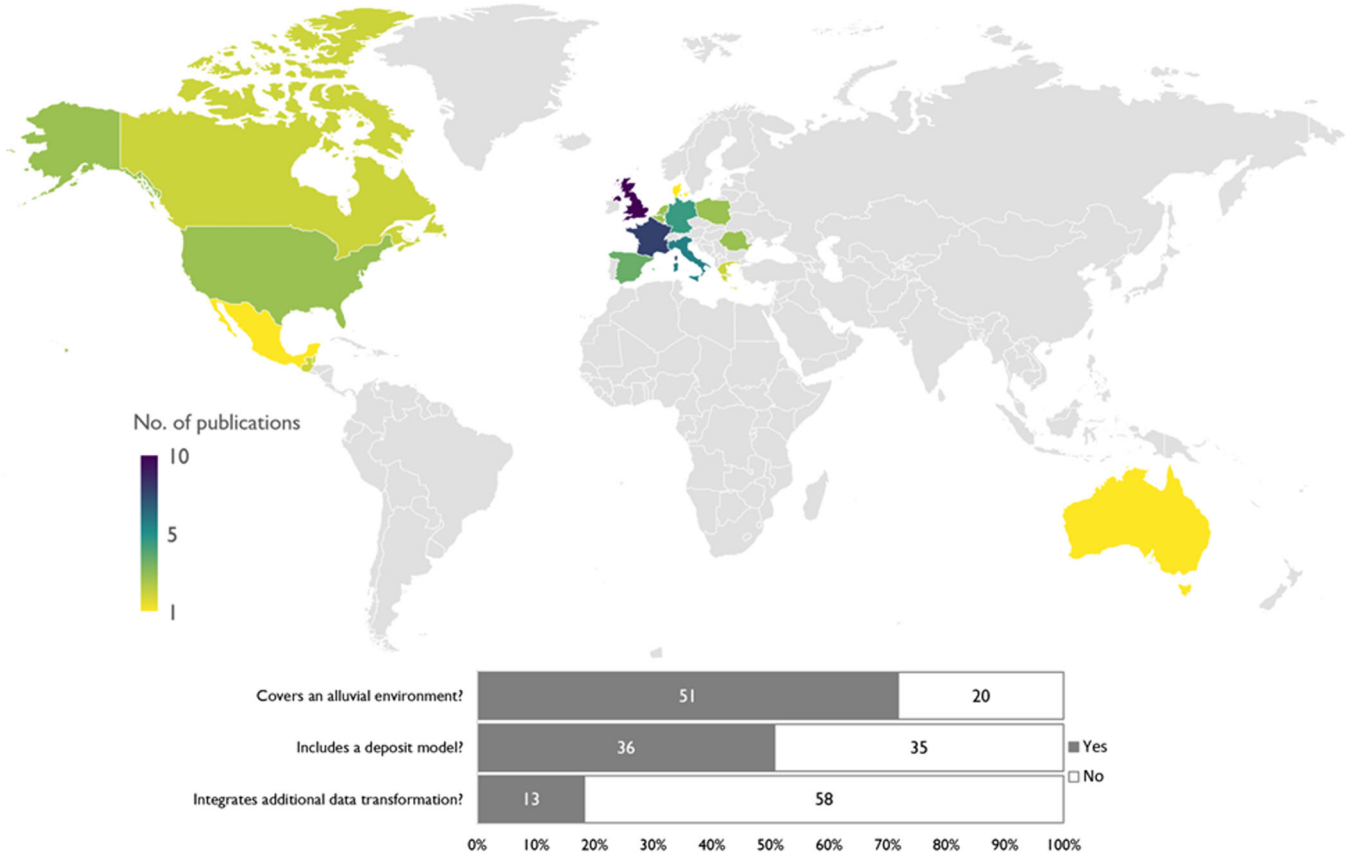

FIGURE 1 Visual summary of existing geoarchaeological literature that integrates lidar as part of their methodology. The term deposit model is applied in its broadest sense (e.g., the distribution of buried deposits of geoarchaeological interest is mapped across a site or landscape) and additional data transformations refer to any visualization method applied, beyond the simple display of an unaltered DEM. The total number of publications identified was 71 and full details are available in the table provided as Supporting Information Material. DEM, Digital Elevation Models.

hemisphere (Figure 1). This is partly due to the accessibility of national or near-national data coverage within these areas at a relatively high spatial resolution (0.5–2 m), which has led to the wide use of these data sets to study the topographic expression of archaeological remains and natural landforms that can contain significant archaeological and palaeoenvironmental archives (e.g., Crutchley & Crow, 2010; Höfle & Rutzinger, 2011; A. F. Jones et al., 2007; Notebaert et al., 2009; Opitz & Cowley, 2013). Beyond this, numerous geoarchaeological projects have also used lidar to map geomorphological landforms within alluvial environments to model the distribution of archaeological resources (Brunning & Farr-Cox, 2005; Carey et al., 2017; Challis, 2006; Challis & Howard, 2006; Challis, Carey, et al., 2011; Stein et al., 2017). However, alongside simply applying lidar topography to map and model landforms and archaeology, an increasingly diverse range of methods that provide visual enhancements of the topographic models have been developed, allowing for better identification of surface and subsurface features and sediments (Devereux et al., 2008; Hesse, 2016; Kokalj, Zakšek, Oštir, Pehani, et al., 2019; Štular, Lozić, et al., 2021).

Lidar visual enhancement methods vary in complexity and applicability across the full range of landscape settings (e.g., from shallow superficial cover in uplands to deeper sequences found in lowland alluvial and intertidal areas). Within the context of geoarchaeological applications, lidar is commonly used for topographic modelling of landforms of variable archaeological or palaeoenvironmental potential (Corrò & Mozzi, 2017; Mozzi et al., 2018; Ninfo et al., 2011, 2016; Passmore & Waddington, 2009) and given its relatively wide use for geoarchaeological deposit modelling, it is timely to provide a more thorough evaluation of visualization techniques that are most effective for this purpose. Moreover, alluvial environments offer a unique and challenging setting, where consideration of these visual enhancement techniques is of specific importance for the enhancement of subtle geomorphological features and associated modelling of their archaeological potential.

2 | LIDAR FUNDAMENTALS

Lidar (Light Detection and Ranging) is an active form of remote sensing that uses pulses of laser light to measure distances to the earth's surface. Most lidar systems operate using very narrow beams of laser (NIR) light (typically 1064 nm) and are operated from airborne platforms, though there is an increasing array of UAV-mounted

(drone) sensors and terrestrial laser scanners that have been used for archaeological research and a variety of Earth observation applications (Pádua et al., 2017; Telling et al., 2017). However, this paper is principally concerned with airborne laser scanning and its geoarchaeological application within temperate alluvial environments.

Lidar is typically acquired as discrete return or full-waveform data, which are then converted into a point cloud. Discrete return data record information only from targets that yield strong returns over a predefined threshold, whereas in full-waveform data, the whole waveform is practically digitized, regardless of intensity or strength, to provide a vertical profile over time (Melin et al., 2017). Discrete return data sets are most common and are sufficient for most geoarchaeological applications but full-waveform data may offer some distinct advantages, particularly in densely vegetated areas, where it can increase the number of data points derived from the ground surface (Doneus et al., 2008; Lasaponara et al., 2011; Stott et al., 2015) while also informing understanding of vertical structure (Brolly et al., 2016).

2.1 | Data acquisition

Lidar data sets have been extensively collected by national governmental survey agencies and research institutions, many of which are freely available, providing an exceptional resource for geoarchaeological and archaeological projects. An extensive list of agencies or organizations that provide access to these lidar data sets can be found in Melin et al. (2017) and Kokalj and Hesse (2017). In England, the Environment Agency's National Lidar Programme (NLP) provides high spatial resolution (0.5–2 m) elevation data for most of the country (Environment Agency, 2021). Surveys are principally undertaken during the winter months and are available as Open Government license data, which can be downloaded from the DEFRA Data Services Platform as point cloud and rasters (Department for Environment Food and Rural Affairs, 2021).

For projects that integrate airborne lidar collected by government agencies, the choice of instrumentation or data collection parameters is predetermined and, as a result, in some cases, it can be beneficial to commission a bespoke lidar survey from a private company, when specific data acquisition is required. Whilst this can be expensive, as with most technologies, this type of data is becoming more affordable (Bluesky International Ltd., 2022). The cost of lightweight lidar sensors that can be mounted on UAV systems (drones) is also coming down, but these range from survey-grade instruments to repurposed sensors originally designed for the automotive industry. As the characteristics of these instruments vary, numerous data acquisition parameters require consideration to ensure their effective use, including range accuracy, beam divergence (footprint size and shape), wavelength, number of returns recorded and accuracy of the GPS and IMU (Kellner et al., 2019). There are also numerous complexities surrounding mission planning and subsequent data processing to ensure the generation of accurate terrain models (Casana et al., 2021). However, archaeological applications of this technology are increasing and perform well in a variety of conditions (Casana et al., 2021; Risbøl & Gustavsen, 2018; van Valkenburgh et al., 2020). The main advantages are the increased flexibility, low flight altitudes, small laser footprint and the advantages of a far-reaching field of view, which ultimately enable a higher point-cloud density (Risbøl & Gustavsen, 2018). Previous research has also shown that this higher spatial resolution enables an improved definition of the physical properties of topography (Resop et al., 2019). This may also provide improved capabilities within wooded environments, but since most sensors provide discrete return rather than full waveform data, this may be relatively limited, as only a small number of the last returns may relate to the ground.

2.2 | Standards and guidance

There is currently no standard approach to the integration of lidar in archaeological practice but there are several overviews of approaches to airborne data (Crutchley & Crow, 2010; Historic England, 2018; Kokalj & Hesse, 2017; Opitz & Cowley, 2013). The Europae Archaeologiae Consilium (EAC) Remote Sensing Working Group is, however, currently preparing guidelines for the use of lidar in heritage management across Europe, which is due to be published in 2024 (Europae Archaeologiae Consilium, 2022). In addition, a recent research article has provided a comprehensive review of archaeology-specific workflows for airborne lidar data acquisition, processing and interpretation (Lozić & Štular, 2021). This highlights a series of common steps and sub-processes centred around point-cloud processing and derivation of products, followed by archaeological interpretation, dissemination and archiving. However, the specific considerations and workflow of each project will depend on the nature of the landscape in question and whether it involves commissioning the acquisition of new data or integration of existing data.

2.3 | Data products

Regardless of whether lidar data are captured from an airborne or UAV-based platform, the primary data set for lidar is a point cloud, which comprises information regarding the *X*, *Y* and *Z* coordinates of the returns and additional attribute information such as GPS time, intensity and scanning angle (Lozić & Štular, 2021). These points can be classified into different object types such as ground, low, medium and high vegetation classes using an automated or manual process (Štular, Eichert, et al., 2021), although manual classifications are rarely done on a large scale. Ideally, point-cloud data will be provided in a.LAZ format, which must be decompressed into a.LAS format for use within GIS software. These files are not always available, can be very large and can be efficiently converted through the open-source LAZ converter provided by LAStools (rapidlasso GmbH, 2021). These data can then be used in the creation of different DEMs. Point-cloud data allow the data quality and effectiveness of the classification to be

interrogated/checked (Kokalj & Oštir, 2018; White, 2013). They also enable the gridding of Digital Surface Models (DSMs) and Digital Terrain Models (DTMs) by only considering the first and last returns, but preprepared DSMs and DTMs can also be downloaded in a standard ASCII format.

DSMs are created from the lidar pulses returned to the sensor relating to all ground surface objects, whereas DTMs are created from the last return classified as ground by filtering out surface objects (Environment Agency, 2021). For the DTM, manual filtering can also be undertaken to improve the automated classification routines and produce the most likely ground surface model. While surface objects such as modern buildings and vegetation are useful to orientate data in the landscape, they can be distracting for palaeolandscape reconstructions associated with geoarchaeological deposit models and DTMs are, therefore, most extensively used, as this provides a refined bare earth (ground) model. The intensity data for each area can also be used to provide a measure of the amount of laser light from each laser pulse reflecting from an object (Environment Agency, 2021). This reflectivity is a function of the near-infrared wavelength used and the material incident upon, but also the angle of incidence, flight altitude and the number of returns that can be used as a proxy to analyse the reflectivity of the surface (Historic England, 2018). Although previous applications of these data within an alluvial context have proved inconclusive, it can aid interpretation, particularly relating to the location of organic and waterlogged deposits (Challis et al., 2008),

2.4 | Processing software and tools

Lidar data can be processed through a variety of proprietary or open-source GIS and remote sensing software (e.g., ArcGIS, ENVI, GRASS, SAGA and QGIS). These enable the generation of standard lidar products from the original point-cloud data and there are numerous tutorials and guides available (e.g., Davis, 2012). In addition, numerous visualization methods are also integrated or can be installed as an additional plugin but some methods may require bespoke model building or equations. Given that most geoarchaeologists will be familiar with GIS, this is perhaps the most convenient environment for processing lidar data. In addition, there are freely available toolboxes (e.g. RVT, LiVT and Whitebox tools) that are dedicated to the production of lidar visualizations and facilitate a wide range of advanced visualization procedures (Hesse, 2013; Kokalj, Zakšek, Oštir, Pehani, et al., 2013).

3 | CONTEMPORARY APPROACHES TO LIDAR VISUALIZATION

Lidar-derived DEMs can be difficult to interpret in their raw data form but visualization techniques can be used to improve the definition of features of interest or transform the data into other physical quantities such as degree of slope or aspect (Kokalj & Hesse, 2017). While the simple visualization of lidar data within standard GIS software converts the original data into new values by applying a histogram stretch that distorts but does not store the original data, other visualizations transform the data values, which can then be stored as a new independent raster data set. A growing number of these transformation techniques that vary significantly in complexity but can be broadly grouped into three categories that use similar approaches are provided as follows:

1. Illumination techniques.
2. Topographic filtering.
3. Blending.

While there have been several empirical assessments of these techniques (e.g. Bennett et al., 2012; Challis et al., 2011b; Devereux et al., 2008; Štular et al., 2012; Thompson, 2020), it can be very difficult to establish the most appropriate technique for a particular site or landscape. There has also been a small number of more objective evaluations for a limited range of archaeological features (e.g., field systems and burial monuments) and landforms such as palaeochannels and landslide scars (Guyot et al., 2021; Mayoral et al., 2017; Notebaert et al., 2009) and when new visualization methods are proposed, they are normally assessed in relation to pre-existing approaches (e.g., Doneus, 2013; Hesse, 2010; Orengo & Petrie, 2018; Zakšek et al., 2011). However, the results of these studies have emphasized that there is no single visualization, or combination of visualizations, that consistently performs well in all situations. Despite this, it is often possible to identify techniques that are most suited to specific types of terrain. For example, Local Relief Models (LRMs) are commonly found to perform well in low-relief areas, whereas the Sky-View factor may be more appropriate in areas of steeper ground (Kokalj, Zakšek, Oštir, Pehani, et al., 2019; Mayoral et al., 2017).

Since alluvial landscapes contain rich archaeological records closely linked to a range of landform assemblages, it is challenging to select appropriate visualization methods that can enhance the visibility of the full range of resources that are potentially present. Many of the approaches to lidar visualization are designed to highlight small-scale archaeological features, but larger-scale natural landforms such as broad palaeochannels, levees and gravel islands may only exist as slight topographic variations that extend over hundreds of metres (Orengo & Petrie, 2018). As such, there is a need to establish which techniques are most appropriate for the identification of geoarchaeological features within alluvial environments, as well as consider how they might be integrated within a deposit modelling framework. The remainder of this paper provides an overview and quantitative evaluation of a range of commonly used lidar visualization techniques in archaeology and geomorphology and highlights those that are likely to be most applicable from a geoarchaeological perspective.

3.1 | What makes a good visualization?

Within geoarchaeological deposit modelling, the purpose of using lidar is to define the surface expressions of geomorphological

landforms and relate these to more deeply buried deposits of geoarchaeological interest across a site or landscape, which can then be interpreted in terms of their archaeological and palaeoenvironmental potential. In essence, this is not dissimilar to archaeologists working in dryland environments to identify topographic features associated with past human activity or geomorphologists studying landforms and landscape evolution; rather, it is a combination of the two. However, as discussed, the physical shape and extent of archaeological features and geomorphological landforms are very different, ranging from small to large scale. Consequently, effective geoarchaeological visualizations need to account for this wider range of different feature types.

More generally, the visualization of lidar data should follow good practice principles required for any cartographic or raster data set (e.g., Borland & Taylor Ii, 2007). Grey or colour scales should be easily understandable and representative of the order of data (Kirk, 2019). However, if the data values have a zero point, a dichromatic scale may be more appropriate to emphasize deviation from this (Campbell & Shin, 2011). It is also sometimes useful to use pseudo-realistic multipart colour schemes, but the number of contingent colours should not be excessive so that they cause confusion. Some colour scales, such as rainbow palettes, should be avoided as their nonsequential luminosity intensities can introduce false borders or artefacts in the data (Kokalj & Somrak, 2019).

Beyond increasing image contrast for the human perception of archaeological features and natural landforms, lidar visualizations are also utilized to improve automated, or semiautomated, object detection (Davis, 2019; Verschoof-van der Vaart & Lambers, 2022). In geomorphology, these procedures are increasingly critical for providing a quantification and recognition of landforms that possess unique morphometric characteristics (Evans, 2012; Jasiewicz & Stepinski, 2013; Lin et al., 2021; Wang et al., 2010). In archaeology, the focus of these procedures has also been more restricted to the detection of morphologically distinct features such as pits, linear features, mounds and other structures (e.g., Cerrillo-Cuenca, 2017; Freeland et al., 2016; Niculiță, 2020; Schneider et al., 2015; Trier & Pilø, 2012). However, algorithms for multiple and more complex feature types are increasingly being developed, particularly through the application of deep learning techniques such as convolutional neural networks (Bonhage et al., 2021; Bundzel et al., 2020; Meyer et al., 2019; Trier et al., 2019, 2021; Verschoof-van der Vaart & Lambers, 2019; Verschoof-van der Vaart et al., 2020). As such, some visualizations are targeted toward ensuring that the broadest range of features is detectable by combining optimal aspects of various techniques (Guyot et al., 2021; Kokalj & Somrak, 2019). However, there is no agreement in terms of which visualization methods produce the best results for these approaches. Despite this, the principles of what makes a good visualization are largely the same, regardless of whether it is produced for an automated or manual interpretation. Thus, although this study does not attempt any automated procedures, the considerations presented here are important for any future research that may aim to utilize these methods within an alluvial setting.

The default visualization of raster data sets within GIS software is a linear grey scale, with black denoting low values and white defining high values. A very simple method of improving the contrast of this is to constrain the image to a more appropriate data range, which can be achieved using a linear histogram stretch or manual saturation of extreme values (e.g., identifying the mean and range of elevation values contained within an area of interest such as a flood plain). 'Elevation' colour ramps are also widely used as they are very intuitive, where light blue relates to low-lying positions and darker red and white relate to higher areas. However, where the overall topography deviates from horizontal, it can be difficult to select the optimal elevation range for the full suite of landforms within a flood plain (Kokalj & Hesse, 2017).

One approach to overcoming the issue of identifying effective elevation ranges was developed by A. F. Jones et al. (2007). This comprised classifying multiple elevation ranges to enable the visualization of different landforms at different intervals (e.g., 4, 2, 1, 0.5 m, etc). This approach allowed the delineation of both large features, such as prominent terrace edges, and subtle features, such as shallow palaeochannels, which were mapped sequentially depending on the range of these intervals. Whilst this approach was successful, it also highlights the fundamental issue with such visualizations: that it is difficult to characterize the full range of features contained within a DTM of the flood plain using a single image. Moreover, it is also still subject to numerous biases of the landscape such as the inherited form and morphology of the flood plain profile and downstream slope.

3.2 | Illumination techniques

A wide range of image enhancement techniques has been developed for lidar, many of which explore the interaction between the landscape and a hypothetical light source (summarized in Figure 2). The best known and well established of these is hillshading, where each cell is assigned a value (or shading) based on the illumination at a specified azimuth and elevation angle. Areas perpendicular to the light beam are most illuminated, while areas with an incidence angle equal to or greater than 90° are dark (Kokalj & Hesse, 2017). Under very low light source angles (below 10°), more subtle features are enhanced but the use of a single illumination can be problematic for any features that are aligned parallel with the light source (Davis, 2012). To overcome this, different illumination angles can be produced from multiple directions and displayed as an RGB composite image (Devereux et al., 2008). Then, Principal Components Analysis (PCA) can also be used to summarize the variance contained across these multiple (>3) hillshade directions (Crutchley & Crow, 2010). Within such images, high levels of the original data set variance are accounted for within the first three components (*c.* 99%), meaning that the first three-component bands presented as a false colour composite can be an extremely effective way of reducing data dimensionality.

Alternative illumination techniques such as Sky-view factor (SVF) and openness can also be used to overcome the directional problems

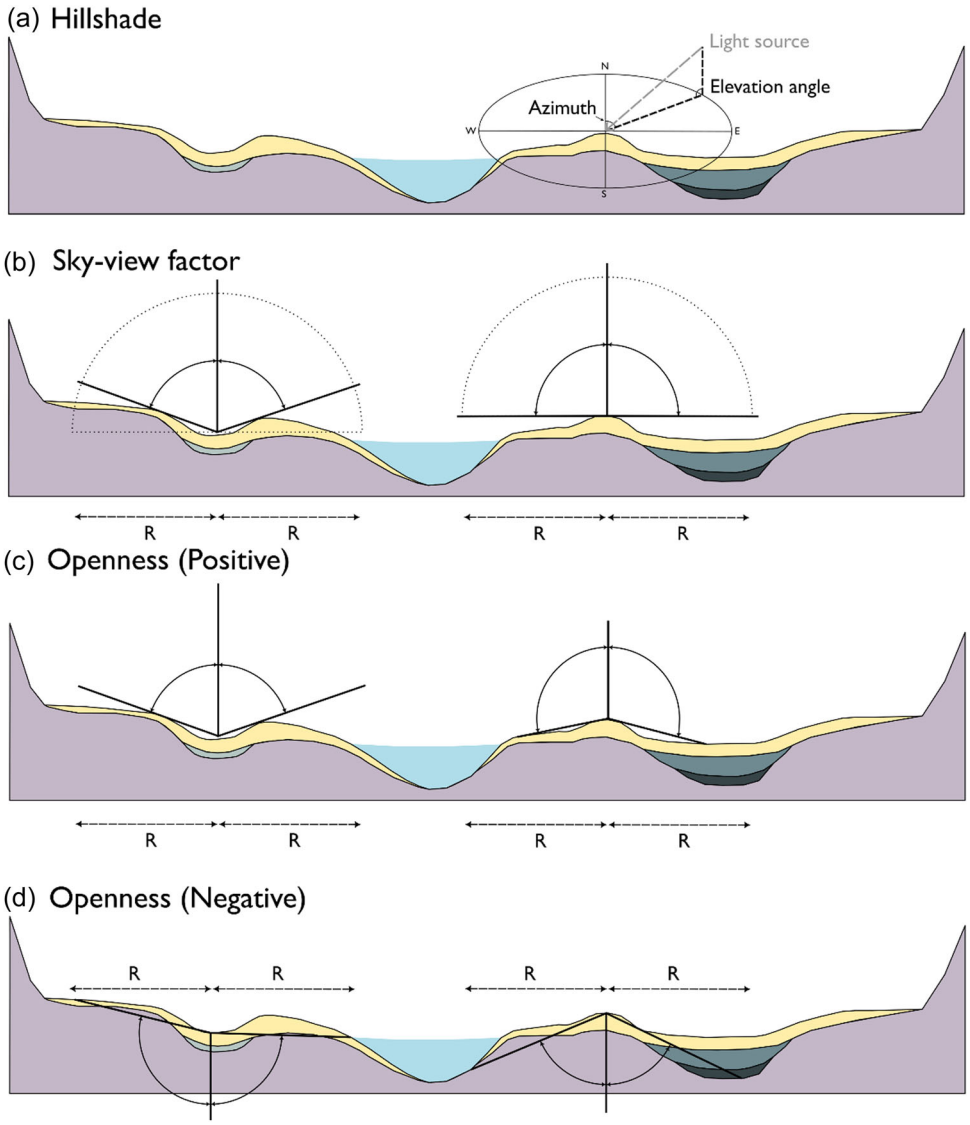

FIGURE 2 Comparison of the calculation principles of illumination techniques for a typical flood plain profile including (a) hillshading, (b) Sky-view factor, (c) positive openness and (d) negative openness (Adapted from Hesse, 2016). R, search radius and colours denote hypothetical sediment units.

of hillshading (Kokalj & Hesse, 2017). Both techniques involve calculating the proportion of visible sky above (or below, as for negative openness) a certain observation point by computing the horizon angle in different directions to a specified radius (e.g., 10–20 m) (Kokalj & Hesse, 2017; Yokoyama et al., 2002; Zakšek et al., 2011). Openness can be provided in a positive (OPP) and negative (OPN) format, where the mean value of all zenith angles gives positive openness and the mean nadir value gives negative openness (Figure 2). Positive openness is similar to Sky-view factor, while negative openness gives additional information on convex features (Doneus, 2013). These techniques provide good general visualizations because they enhance the visibility of simple and complex small-scale features, regardless of their orientation and shape, on most types of terrain (Kokalj, Zakšek, Oštir, 2013).

3.3 | Topographic filtering

Topographic filtering methods attempt to remove the influence of wider topographic trends or convert elevation values into other variables (Figure 3). Many of these are targeted toward the investigation of terrain and landform properties and are widely integrated within commercial GIS software and other open-source tools (e.g., Whitebox tools; Szypuła, 2017). These also enable landform classifications (e.g., De Reu et al., 2013; Jasiewicz & Stepinski, 2013) or specific hydrological or morphometric characteristics to be defined (Gomez-Heras et al., 2019). While they are not all relevant for geoarchaeological research, some are highly applicable for the visualization of low-relief variations associated with landforms and archaeological features.

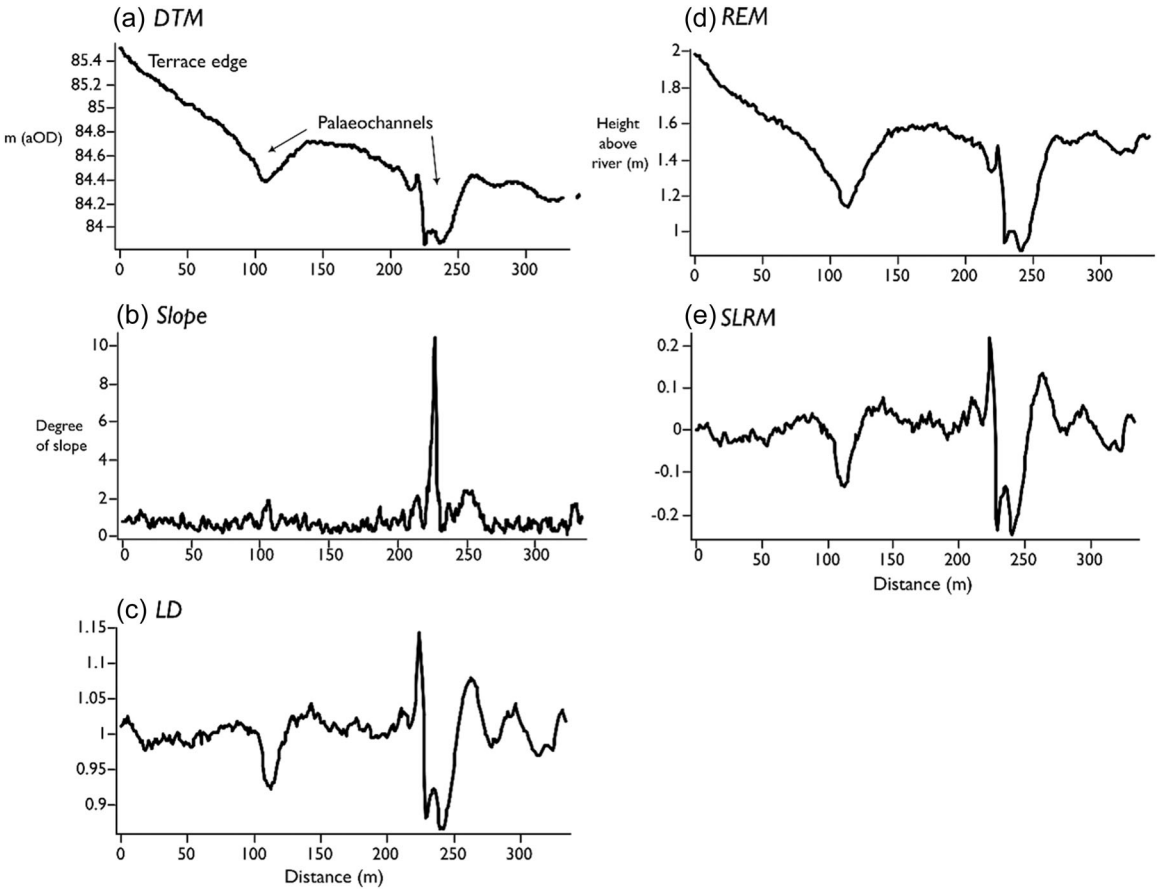

FIGURE 3 Comparison of the effects of topographic filtering on the original Digital Terrain Models (DTM) (a) using slope gradient (b), the Local Dominance (c), the Relative Elevation Model (d) and Simple Local Relief Model (SLRM) for a downslope profile derived from a portion of the Middle Lugg flood plain.

Slope models calculate the slope severity for each cell (calculated as the degree of slope) and darker shades typically represent more steeply sloping areas, with lighter areas corresponding to flatter terrain (Smith & Clark, 2005). Challis et al. (2011b) found slope gradient as the best visualization technique for the identification of most archaeological resources in a flood plain setting. However, a limitation of this method is that it is difficult to distinguish between convex and concave features, as slopes of the same gradient are presented with the same colour regardless of whether they are inclined or declined (Kokalj & Hesse, 2017).

Other topographic filters such as Local Dominance (LD) and Local Relief Models (LRM) attempt to remove the influence of broad topographic trends to highlight more localized variations. Within LD images, the brightness of each pixel corresponds to the mean angle from which a virtual observer looks within a given radius, giving an impression of how a pixel dominates its local surroundings (Hesse, 2016). Simple Local Relief Models (SLRM) are very similar to Local Dominance but apply a low-pass filter to the original DEM, which provides a smoothed version only showing large-scale landscape forms. This is then subtracted from the original DEM to enhance small-scale features. Within a full LRM, a further processing step is applied where a purged DEM is created from the zero-metre contour lines in the SLRM, which is then subtracted from the original DEM to create a less biased elevation of small-scale features than the SLRM, as the elevations of features are relative to the surrounding landscape. However, the SLRM is faster to compute than LRMs and the visibility of the features of interest remains (Trier et al., 2021). In general, these techniques are well suited for very subtle positive relief features such as former upstanding field boundaries and slight depressions such as infilled ditches (Kokalj & Hesse, 2017). They have also been shown to be well suited to areas of relatively flat topography (Kokalj & Hesse, 2017; Mayoral et al., 2017) and are often preferred for the automated detection of archaeological features (Trier et al., 2021; Verschoof-van der Vaart & Lambers, 2019; Verschoof-van der Vaart et al., 2020), although there is rarely explicit justification for their selection over other methods.

An increasingly popular filtering method in geomorphological research is Relative Elevation Models (REMs), which were developed to facilitate examination to delineate fluvial processes and channel migration (Coe, 2022; Notebaert et al., 2009). They are sometimes referred to as Height Above River (HAR) models as they normalize the elevation of the active river channel by creating a detrended DEM and subtracting it from the original data set. REMs can be created using several different methods, including using bespoke

cross-sections of the flood plain (J. L. Jones, 2006) or smoothing algorithms such as Kernel Density (Dilts et al., 2010) and Inverse Distance Weighting (IDW) (Olson et al., 2014). However, the principles behind the process are essentially the same, whereby the DEM is detrended by using the water surface of the present river channels to remove the influence of the downstream slope. In the IDW method, the analysis involves first extracting elevations along the channel to generate a detrended DEM using the IDW tool (Olson et al., 2014). Finally, the detrended DEM is subtracted from the original DEM, resulting in elevation values relative to the water surface of the channel. This produces positive values, except where there are low-lying zones (below the height of the river) within the flood plain. This has obvious merits for identifying upstanding alluvial landforms that may have a high archaeological potential (e.g., gravel islands or terraces) as any elevated parts of the flood plain will be more readily apparent.

3.4 | Blending

There have been several attempts to capitalize on the relative advantages of multiple techniques through image fusion and allow for the simultaneous display of distinct topographical features in a single (enhanced) image (Kokalj & Somrak, 2019). This is potentially less onerous than a manual or automated interpretation of multiple images, but it can be difficult to identify exactly what topographic characteristics are displayed within the resulting visualizations.

Kokalj and Somrak (2019) developed a specific Visualization for Archaeological Topography (VAT) using blending techniques to combine hillshading, slope, positive openness and sky-view factor. It includes options for 'normal', complex and very flat terrain and can be very effective for small-scale features or local geomorphological characteristics, but larger-scale topographic variations that might relate to alluvial landforms may not be well represented (Guyot et al., 2021).

Another blending technique is Red Relief Image Maps (RRIMs), which were developed by Chiba et al. (2008) to overcome the limitations of openness by combining it with a slope gradient. To achieve this, positive openness (OPP) and negative openness (OPN) are combined using the following formula, which is sometimes referred to as the *I*-factor;

$$I = \frac{\mathrm{OPP} - \mathrm{OPN}}{2}.$$

The slope image is then presented in a red-colour scale and overlaid on top of the *I*-factor images using transparencies. This aims to simultaneously highlight morphological features and broad and small-scale topographic features. However, the performance of the *I*-factor is often poor when compared with other techniques (Mayoral et al., 2017).

To overcome the scale-dependent disadvantages of many lidar visualization techniques, Lindsay et al. (2015), developed the Multi-scale Topographic Position (MSTP). This was primarily designed for geomorphological research but has recently been adapted for archaeological applications (Danese et al., 2022; Guyot et al., 2018, 2021). It combines metrics relating to the deviation from mean elevation (DEV) calculated at multiple scales (micro, meso and macro) from roving windows of different sizes between a predefined range for each scale at incremental steps. The size of the window is determined by the size of the features of interest and the incremental step can be set to avoid excessive calculations, with the resulting three DEV combined within a colour-composite or MSTP image (Guyot et al., 2018; Lindsay et al., 2015). These have been objectively shown to perform extremely well in a range of settings (Guyot et al., 2021) but can produce high-contrast images that may be difficult to interpret without a detailed understanding of the technique and its input parameters.

3.5 | Visualization of archaeological resources in alluvial environments

Each of the above visualization techniques has advantages and disadvantages, and some are more appropriate than others for the study of geoarchaeological resources in alluvial environments. For example, some methods are known to be effective over low-relief terrain (e.g., SLRM) or are specifically designed for use within flood plain settings (REM). However, it is impractical and time-consuming to interpret multiple lidar visualizations, particularly when many of the techniques repeat the same information, highlighting features to a slightly different degree. While the use of blending techniques can be used to overcome this issue, the resultant images are often unintuitive for nonspecialists and difficult to relate to the topographic characteristics they were originally derived from. Consequently, it is useful to identify a smaller set of demonstrably effective image-enhancement techniques for use within geoarchaeological projects. To achieve this, a quantitative evaluation has been undertaken for a series of landforms identified within the Lugg and Wye Valleys of Herefordshire, UK. This is combined with qualitative statements and a discussion of their applicability and potential integration with geoarchaeological deposit models.

4 | MATERIALS AND METHODS

4.1 | The Lugg and Wye Valleys, Herefordshire, UK

The Lugg and Wye Valleys were selected for this analysis as they represent typical lowland flood plain settings within the temperate zone, and have been a recent focus for investigating the application of hyper- and multi-spectral data sets within an alluvial geoarchaeology context (Crabb et al., 2022). Both river systems have complex depositional histories, with closely related human–environmental interactions demonstrated by a palimpsest of archaeological records, which have been the focus of previous geoarchaeological

investigations (Brown et al., 2005; Carey et al., 2017; Dinn & Roseff, 1992; Hemingway & Dinn, 1996; Jackson & Miller, 2011; Pears et al., 2020). This has established secure chronostratigraphic knowledge of the landform assemblages, in turn aiding geoprospection at a reach scale, which may be tentatively applied more widely. The specific study areas comprise sections of the Middle and Lower Lugg and the Middle Wye Valleys (Figure 4), each containing a range of alluvial landforms to enable the assessment of lidar visualization.

4.2 | Lidar data

The lidar data used in this analysis were downloaded as 5 × 5 km tiles from the UK Environment Agency NLP (Department for Environment Food and Rural Affairs, 2021). These use the last return data, selected by automated algorithms and manual editing to produce terrain models (UK Environment Agency). The elevation values are recorded in metres above Ordnance Datum Newlyn (aOD) with a vertical accuracy of ±0.15 m, which are then outputted to a DTM with a resolution of 1 m. Where necessary, they were combined to create single mosaics in ArcGIS, covering each study area (Davis, 2012).

4.3 | Calculation of lidar visualizations

In total, 16 different visualizations have been calculated for each of the study areas. These have been created using the Relief Visualization Toolbox (RVT) or ArcGIS and associated plugins or toolboxes (Qiusheng, 2022; Whitebox Geospatial Inc). The specific input parameters are provided (Table 1) and wherever possible, they have been optimized for low-relief variations (Kokalj, Zakšek, Oštir, 2013). For many of these, a search radius of 20 pixels was used to transform the data as this helped to enhance many of the features but also preserved some finer details of the palaeochannels, ridge and swale, and levees adjacent to the river. Although a larger operating window (e.g., 50 pixels) may provide better results for extremely large features, this was found to give a 'washed out' appearance to the smaller-scale features.

4.4 | Evaluation of lidar visualizations in alluvial environments

There is no consensus on the best method to evaluate the capability of lidar visualizations and approaches have varied from qualitative assessments of their performance (e.g., the number of features detected; Bennett et al., 2012; Thompson, 2020) to more empirical judgements based on the success of automated interpretation procedures (e.g., Guyot et al., 2021; Mayoral et al., 2017). A small number of studies have evaluated signal-to-noise ratios as a proxy for image contrast (Štular et al., 2012), but there are currently no studies that quantitatively interrogate the effectiveness of different lidar visualizations. However, within passive remote sensing (e.g., multi/hyperspectral imagery), such an undertaking is of principal importance for image classification where the contrast of different Regions of Interest (ROI) can vary significantly across wavelength bands and spectral indices (H. Jones & Vaughan, 2010). The extent to which a feature (or ROI) can be discerned against its surrounding background is referred to as its 'separability' and there are several numeric (distance) measurements that can be deployed to evaluate this (Swain & Davis, 1978).

The main aim of undertaking these separability analyses is to identify optimal images or assess the effectiveness of training data sets for the automatic classification of different land surface types (Tso & Mather, 2009). Even though automated procedures are becoming increasingly commonplace for archaeological applications of lidar data sets (Bennett et al., 2014; Sevara et al., 2016), it is often not clear why certain visualizations are chosen over others. This is potentially because, until relatively recently, the number of available visualization techniques was limited, and therefore such analyses were not required. Moreover, most evaluations of the quality of lidar data are often more concerned with spatial accuracy (Bakuła et al., 2017), registration of features (Arnold et al., 2006), or classification of point clouds (Melin et al., 2017), as opposed to ensuring maximum feature contrast or enhancement. However, given the increasing diversity of lidar visualization techniques and the availability of open-source software tools, it is necessary to consider such issues more rigorously, and separability measurements provide one method of achieving this.

The *M*-statistic is a relatively simple separability metric that calculates the difference between the means (μ) of two ROIs, normalized by the sum of the standard deviation (σ) using the following formula:

$$M = \frac{(\mu_1 - \mu_2)}{(\sigma_1 + \sigma_2)}.$$

This provides a measurement of the separation between the histograms of two classes, with $M > 1.0$ indicating good separability and $M < 1.0$ indicating poor separability (Kaufman & Remer, 1994). As archaeological features and natural landforms are often very subtle, they will typically fall below this threshold, but the metric can still be used as an evaluative tool. Although it does not enable the separability of features within multiband images, their constituent parts (individual RGB bands) can be assessed. While other separability measurements (e.g., JM distance or transformed divergence) are better suited to multiband images, it is difficult to compare the results to the assessment of single-band images provided through the *M*-statistic (Crabb et al., 2022; Richards, 2013). However, in contrast to these and other common statistical analyses of variance and difference (ANOVA/*t* tests), the *M*-statistic does not account for sample size. Although this can influence the results, it is of less concern for larger data sets, as the influence of any outliers is reduced. As such, the *M*-statistic was selected to assess the capability of the 16 visualization techniques undertaken as part of this analysis, but it was ensured that each ROI consisted of >1000 pixels.

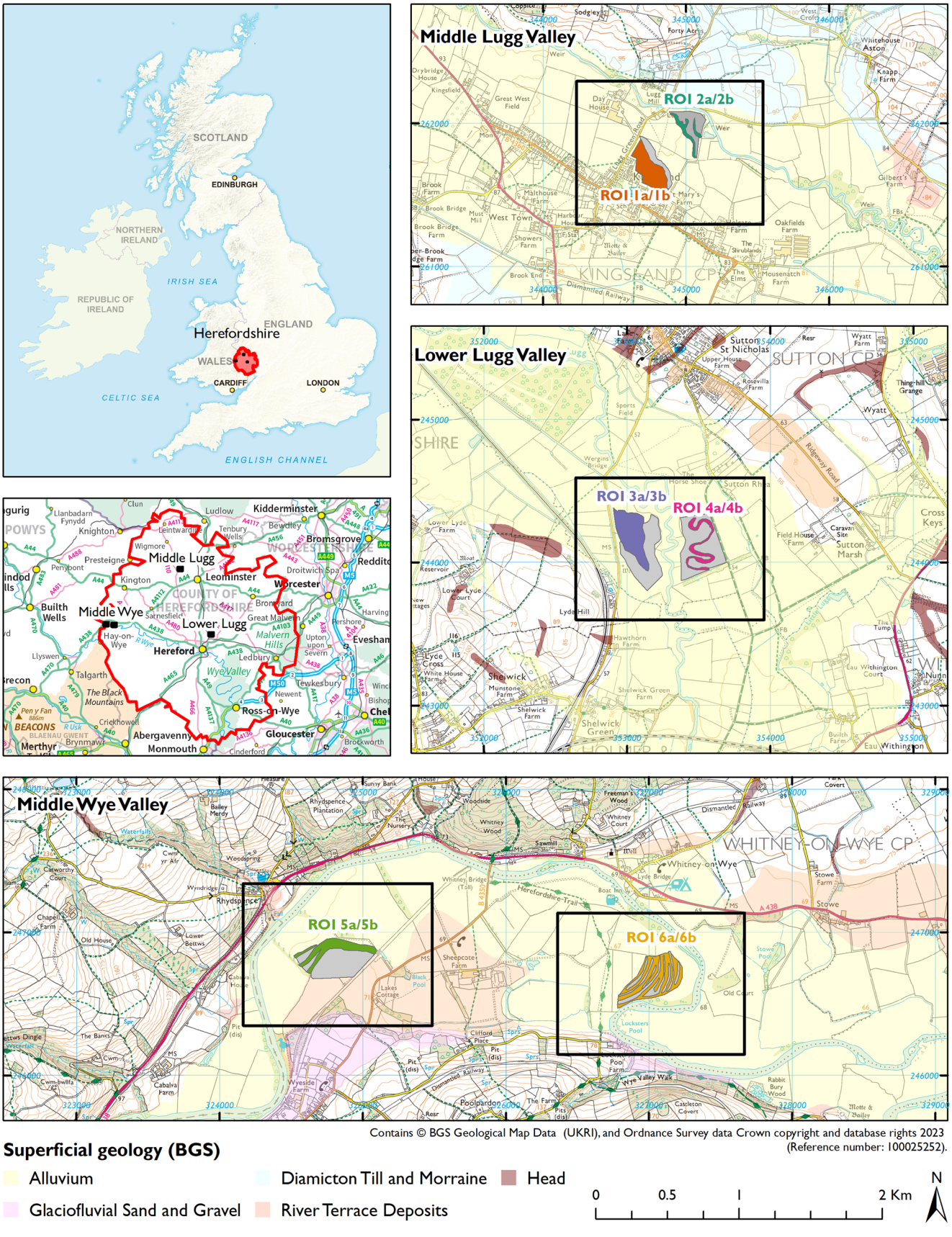

FIGURE 4 Location of Lugg and Wye Valley study areas on a national, regional and local scale, with British Geological Survey (BGS) superficial geological deposits. The colours of the polygons relate to each of the Regions of Interest (ROI) pairs used in this analysis.

TABLE 1 Visualization techniques used in this analysis and their technical properties.

Visualization technique	Acronym	Parameters	Processing software	References	Category
Digital Terrain Model	DTM	Variably constrained to flood plain elevation range	ArcGIS	A. F. Jones et al. (2007)	Illumination techniques
Hillshade (low sun angle)	HSL	Azimuth 315°, Sun elevation angle 10	RVT 2.2.1	Crutchley and Crow (2010)	
Multidirectional Hill shade (RGB)	MD HS	16 azimuth directions, Sun elevation angle: 10	RVT 2.2.1	Devereux et al. (2008)	
		(R = 315, G = 15, B = 75 [60° separation])			
Principal components analysis of multidirectional hillshading	PCA HS	Three principal components (R = PC1, G = PC2, B = PC3)	RVT 2.2.1	Devereux et al. (2008)	
Sky view factor	SVF	Search radius = 20 cells, 16 directions	RVT 2.2.1	Zakšek et al. (2011)	
Openness (positive)	OPP	Search radius = 20 cells, 16 directions	RVT 2.2.1	Doneus (2013)	
Openness (negative)	OPN	Search radius = 20 cells, 16 directions	RVT 2.2.1	Doneus (2013)	
Slope gradient	SLP	No parameters required	RVT 2.2.1	Doneus et al. (2008)	Topographic filtering
Local dominance	LD	Minimum radius = 10, maximum radius = 20	RVT 2.2.1	Hesse (2016)	
Simple Local Relief Model	SLRM	Radius for trend assessment = 20 cells	RVT 2.2.1	Hesse (2010)	
Relative Elevation Model	REM	Detrended DTM using the height of the river.	ArcGIS	Olson et al. (2014)	
Visualization for Archaeological Topography (flat terrain)	VAT	SVF-Blending = Multiply, 25% opacity	RVT 2.2.1	Kokalj and Somrak (2019)	Blending
		OPP-Blending = Overlay, 50% opacity			
		SLP-Blending = Luminosity, 50% opacity			
		HS–Blending = Normal			
Multiscale topographic position	MSTP	*R* = Macro scale (150–1000 cells),	ArcGIS/Whitebox Tools toolbox	Guyot et al. (2018); Lindsay et al. (2015)	
		G = Meso scale (15–150 cells),			
		B = Microscale (1–15 cells)			
Red Relief Image Map	RRIM	Slope (70% opacity)	ArcGIS/RVT 2.2.1	Chiba et al. (2008)	
		I-factor			
Openness *I*-factor	OPIF	*I* = (OPP–OPN)/2	ArcGIS/RVT 2.2.1	Chiba et al. (2008)	

Six ROI pairs were established for evaluation through separability tests, which were derived from the Middle and Lower Lugg valleys and the Middle Wye Valley. These comprise a 'feature', indicated by an 'a', and their surrounding background, indicated by a 'b', from a select sample of typical alluvial landforms (e.g., palaeochannels, gravel islands, ridge, swale, etc.). The features were principally defined topographically and have been subsequently confirmed through boreholes, although the results of this are not reported here. Each ROI was digitized as a polygon and was observable in the original (unaltered) DTM presented in Figure 5. Each ROI pair has been assigned a colour, with the surrounding background response highlighted in grey (Table 2).

5 | RESULTS

Each of the visualizations of the 1 m lidar DTMs is presented in a grid layout to facilitate comparison but are grouped into illumination techniques (Figure 6), topographic filtering (Figure 7), and blending methods (Figure 8). Through empirical observation, it is apparent that palaeochannels are often poorly defined in the original DTM, but are visibly enhanced by topographic filtering, as well as some of the illumination and blending techniques. In addition, most of the larger-scale landforms (e.g., gravel terraces and islands) are less clearly represented by visualization techniques than the original DTM, except for REM, which provides an improved definition. However, it is not possible from a simple visual comparison to establish which technique is most effective.

5.1 | Quantitative assessment

The results of the *M*-statistic calculations are shown in Figures 9 and 10. The cumulative scores in Figure 9 illustrate which visualization methods work best overall, across each of the feature types covered by the study areas. In contrast, Figure 10 shows the variable effectiveness of each technique for these different feature types (ROI). Perhaps one of the clearest and most important aspects of this is that the original (unaltered) DTM provides some of the best separability results of all the visualizations, particularly for larger features. For example, both ROI 3a/3b and 5a/5b produce scores above the threshold ($M > 1$) and 1a/1b is also relatively high. These all represent larger-scale upstanding landforms (e.g., river terraces and gravel islands). In contrast to this, the smaller-scale features such as palaeochannels (ROI 2a/2b and 4a/4b) and ridge and swale (6a/6b) achieve lower separability scores, but the original DTM is by no means the worst-performing visualization analysed.

The best-performing illumination technique is SVF, which provides effective enhancement of the low-lying palaeochannel at ROI 2a/2b and the ridge and swale at 6a/6b. This is also the case for both the positive and negative openness images, with OPP providing a slightly higher score for 6a/6b. However, in general, all the illumination techniques have performed poorly for ROIs located in the Lower Lugg Valley (ROI 3a/3b and 4a/4b), where the magnitude of features is low when compared to the Middle Lugg and Wye Valleys.

Many of the topographic filtering methods have produced comparable M-statistic scores to the SVF and Openness images, but the LD and SLRMs perform slightly better, providing a higher feature contrast for the smaller-scale features (e.g., ROI 2a/2b and

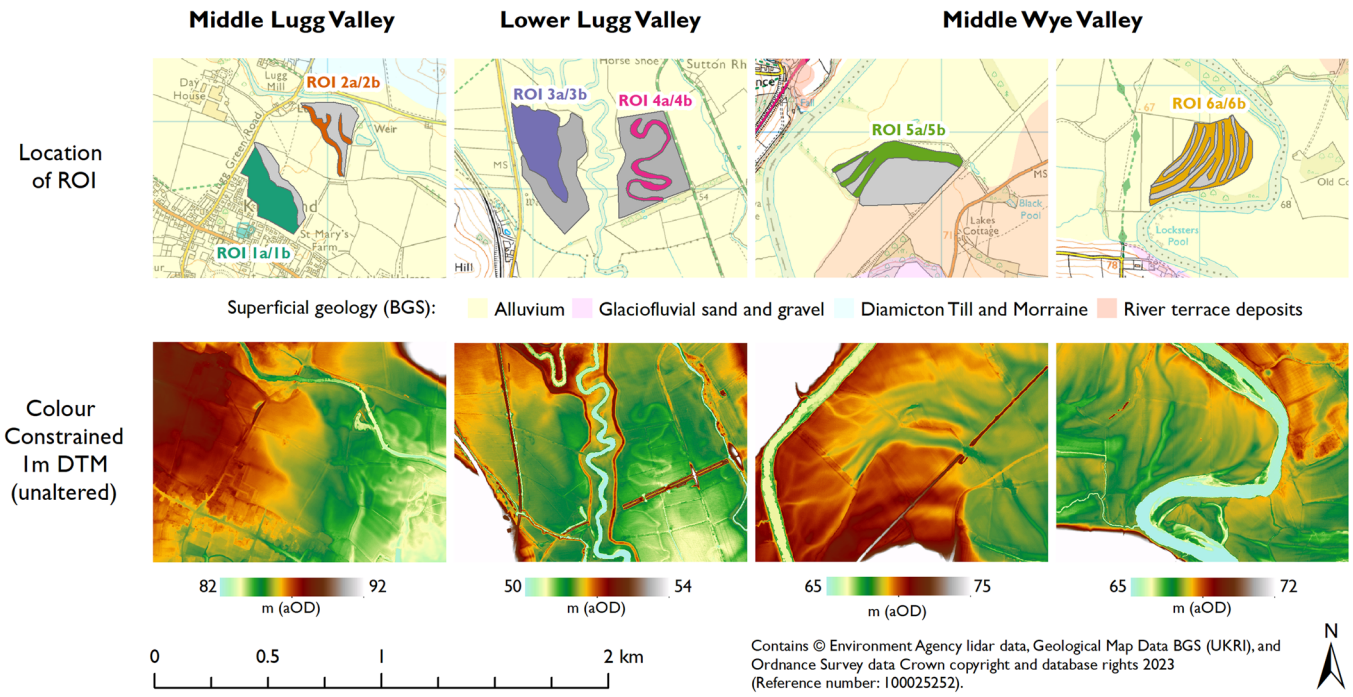

FIGURE 5 Detailed view of ROI pairs derived from the Lugg and Wye Valleys, with recorded superficial deposits and (unaltered) colour-constrained 1 m lidar DTM of each area. DTM, Digital Terrain Model; ROI, Regions of Interest.

TABLE 2 Summary of ROI pairs used for the derivation of statistics for the calculation of the *M*-statistic.

ROI pair	Location	Feature type	Description	Dimensions
1a/1b	Kingsland, Middle Lugg Valley	Gravel terrace/ Palaeochannel	Topographic high point extending north of the village of Kingsland. On the northeast of this, there is a drop in elevation, which was likely formed by former river courses.	Large-scale 4.3 ha *area*. With a broad (50 m+) wide channel.
2a/2b	Kingsland, Middle Lugg Valley	Palaeochannel/background	Sinuous former channels located directly southeast of Lugg Mill. This is located within a wider lower topographic zone adjacent to the present course of the River Lugg.	Palaeochannel measuring c. 20 m wide.
3a/3b	Sutton St Nicholas, Lower Lugg Valley	Gravel island/background	A lenticular topographic highpoint within the centre of the flood plain. This is surrounded by a lower topographic zone, which was likely formed by palaeochannels.	Large 5.7 ha gravel island surrounded by a slightly lower area
4a/4b	Sutton St Nicholas, Lower Lugg Valley	Palaeochannel/background	Highly sinuous former river course, which runs parallel with the present course of the River Lugg. This is surrounded by a homogenous area of flat flood plain.	c. 20 m wide palaeochannel.
5a/5b	Whitney-on-Wye, Middle Wye Valley	Palaeochannel/River terrace	Part of a dense concentration of palaeochannels within a narrow part of the flood plain, directly north of an outcrop of river terrace deposits, which overlooks the flood plain.	Large area of river terrace measuring 7.3 ha and c. 20–30 m wide channels.
6a/6b	Whitney-on-Wye, Middle Wye Valley	Ridge/Swale	A series of curved, arcuate-ridges and depressions (swales) associated with the lateral migration of the present river course. This is located at a tight meander bend of the river.	c. 20–25 m wide ridges with shallow 15–20 m wide depressions.

6a/6b). However, they also work relatively well for some larger-scale landforms, although these do not exceed those achieved by the unaltered DTM.

The slope gradient image does not provide a visual enhancement of most of the ROI pairs, and only the palaeochannel at ROI 2a/2b is improved. In fact, it is less effective than many of the illumination techniques, excluding hillshading.

The best-performing technique of the topographic filters and other visualization types is the REM images. REM produces high separability scores for most of the ROI pairs, with 1a/1b and 5a/5b exceeding the ($M > 1$) threshold. Both of these relate to gravel terraces with adjacent palaeochannels and are associated with large-scale but high-magnitude changes in elevation. Interestingly, it does not provide an improvement for ROI 3a/3b, most likely because the gravel islands are slightly upstanding in comparison with their surrounding topography. All of the smaller-scale features (ROI 2a/2b, 4a/4b, and 6a/6b) also achieved higher separability scores than the original DTM, suggesting that it provides an effective visualization tool for a wide range of resources in alluvial environments.

Most of the images formed via blending methods are more effective than those by illumination techniques but provide lower M-statistic scores than topographic filtering. The combination of both positive and negative openness (*I*-factor) provides a notably improved contrast for smaller-scale features such as ROI 2a/2b and 6a/6b. Similar results were also encountered for the VAT image but in both cases, larger-scale landforms such as ROI 1a/1b, 3a/3b, and 5a/5b are poorly represented.

None of the blending methods achieved M-statistic scores over the ($M > 1$) threshold, but the macro-scale MSTP image for ROI 5a/5b is very close ($M = 0.92$). The microscale MSTP image is one of the worst-performing images, but the meso- and macro-scale images provided an improved definition of the palaeochannels at ROI 2a/2b and 4a/4b. However, it is notable that when combined as a composite image, many of the alluvial landforms are visually very high in contrast (Figure 8).

Aside from REM and the original DTM, the most cumulatively effective visualization across all of the ROI pairs was SLRM. This topographic filtering method provides a clearer delineation of small-scale features but is closely comparable to the other visualization techniques. The remainder of the cumulative *M*-statistic scores reiterate the lower-level effectiveness of illumination techniques within a flood plain setting and also highlight the general poor performance of slope gradient images and some of the MSTP images. This is because these techniques are intended to operate at a wider landscape scale, where there are multiple terrain types and more variable topographic profiles. While these can be very effective in a more diverse landscape, they are evidently less effective in a narrow, low-relief flood plain setting and may, therefore, offer limited benefits for the identification of geoarchaeological resources. However, in scenarios where the flood plain is less constrained, such as the Mississippi (Chamberlain et al., 2020) or Rhine-Meuse Delta (van der Meulen et al., 2020; van Lanen & Pierik, 2019), such multi-scalar approaches may be more effective as there is likely to be significant topographic variability.

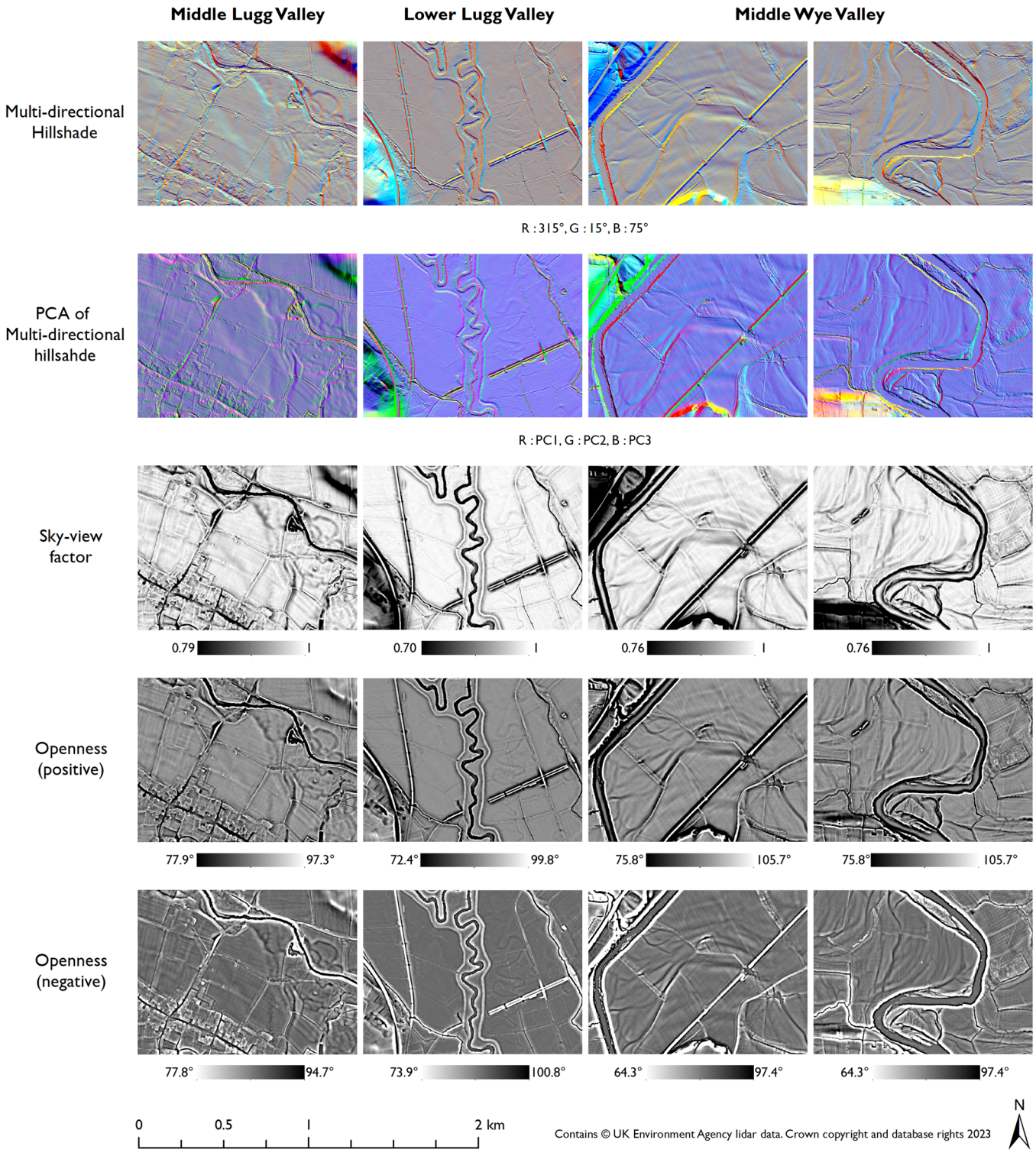

FIGURE 6 Comparison of illumination techniques for each study area.

6 | DISCUSSION

The comparison of lidar visualizations produced for the Lugg and Wye Valleys has shown that an enhanced definition of geomorphological landforms can be achieved using different visualization and transformation techniques. However, the analysis of the *M*-statistic separability tests has shown that only a small number provide a significant improvement over the original, unaltered DTM for the geoarchaeological analysis of alluvial flood plains. The REM image was the only technique that achieved a higher cumulative *M*-statistic score, but where very subtle large-scale landforms are present, the original DTM offered slightly better results. In contrast to this, smaller-scale landforms such as

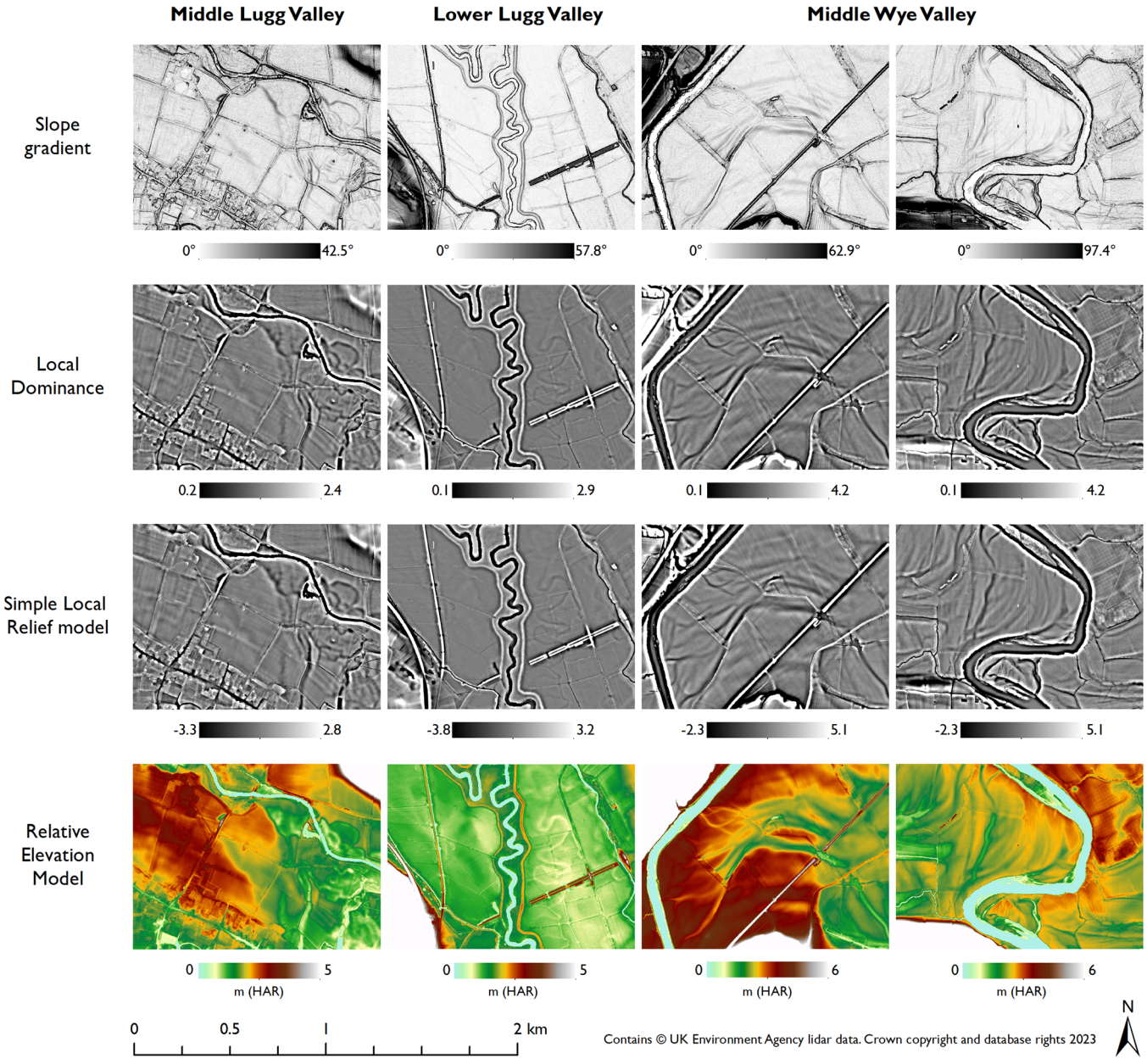

FIGURE 7 Comparison of topographic filtering techniques.

palaeochannels and ridge and swale were better represented by other visualization methods, particularly SLRM. To some extent, these results are expected, as most of these visualization techniques were developed for archaeological purposes to enhance small or low-magnitude earthwork features such as ditches, banks, and other structures (Bennett et al., 2012; Štular et al., 2012). In addition, many of the topographic filters also attempt to reduce the effect of broader topographic trends to enhance localized relief variations (Guyot et al., 2018; Hesse, 2016, 2010). Thus, while this is indeed very effective for small-scale landforms, it has a negative effect on the identification of larger-scale features such as gravel terraces or islands, which are of significant interest within a geoarchaeological context since they are often the focus of settlement and other human activities.

It is challenging to select a single visualization technique that enhances the visibility of every resource that might be present within alluvial environments. This is consistent with previous empirical assessments (e.g., Bennett et al., 2012; Challis, Forlin, et al., 2011; Devereux et al., 2008; Štular et al., 2012; Thompson, 2020) and objective evaluations (Guyot et al., 2021; Mayoral et al., 2017), which have considered a range of terrain types. However, within specific low-lying flood plain settings, with minimal relief, it is possible to make more specific recommendations on which image enhancement techniques produce optimal definitions of geoarchaeological resources, which are summarized in Table 3.

The results of the *M*-statistic separability tests indicate that a combination of REM and SLRM provides the most robust

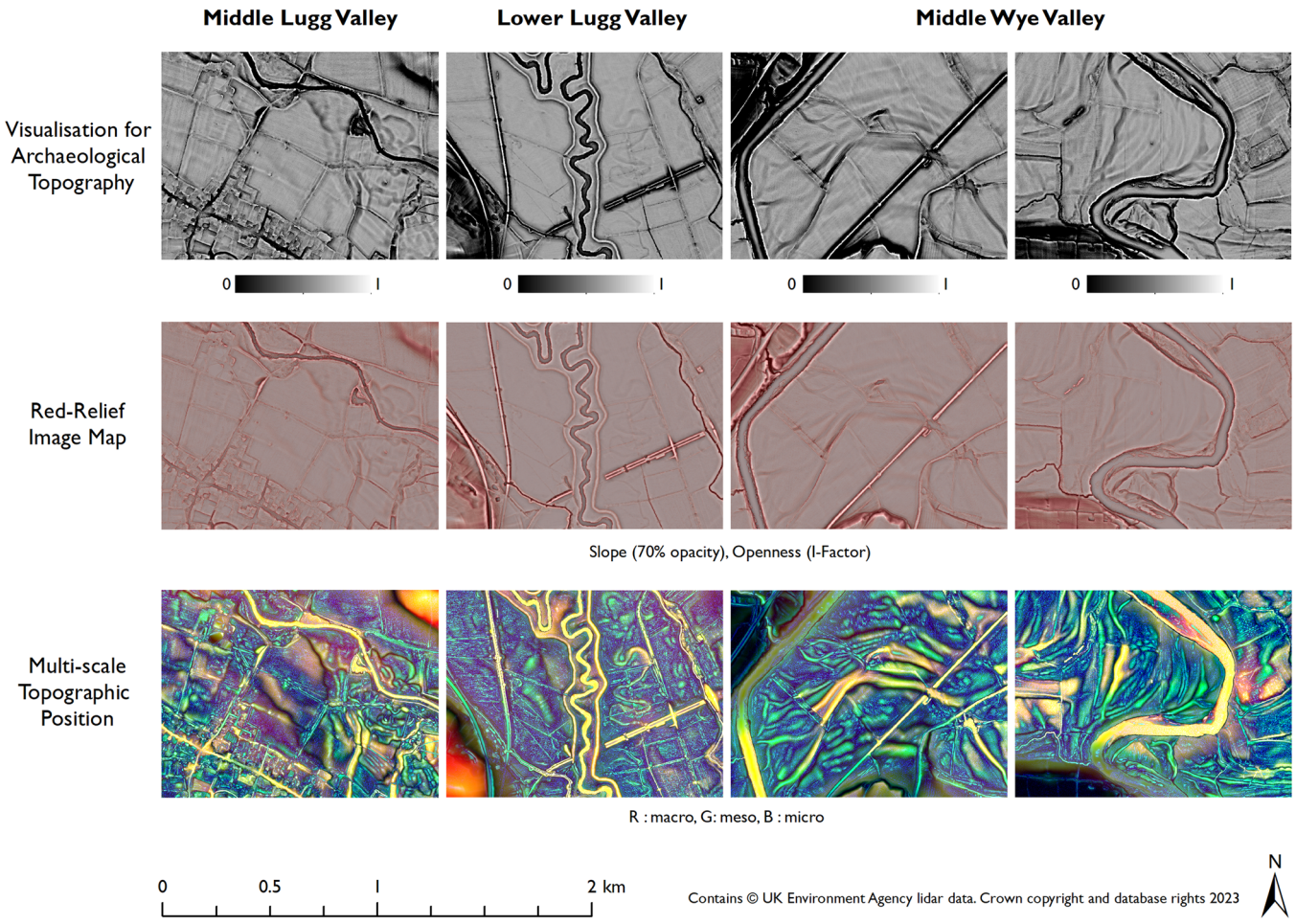

FIGURE 8 Comparison of blending methods.

combination of visualization techniques. As REMs are tools specifically intended to enhance the investigation of geomorphological and hydrographic aspects of river systems (Notebaert et al., 2009; Olson et al., 2014) and SLRM has been previously found to perform well in low-relief areas, (Kokalj, Zakšek, Oštir, Pehani, et al., 2019; Mayoral et al., 2017), these are very appropriate for geoarchaeological research. Consequently, it is feasible to create a new blending technique, capitalizing on the merits of both REM and SLRM, whereby each transformation could be distinguished by colour and luminosity. Such an approach would enable a single image to be interpreted; however, there are advantages in using each image in a separate but complementary manner, as there is more certainty regarding what is being displayed.

Examples of the most effective visualization methods are shown in Figure 11, which highlight the location of the ROI studied here. These data can then be used to create a deposit model for the Lugg and Wye Valleys, where lower-lying (wetter) areas and palaeochannels are more likely to contain palaeoenvironmental resources (e.g. plant macrofossils, pollen, and other ecofactual material), whereas higher (drier) zones, relating to upstanding gravel terraces or islands, will unlikely contain such natural waterlogged remains, but were more attractive for a range of past human activities. These relatively simple statements can also guide the application of subsequent geoarchaeological procedures and/or archaeological mitigation strategies by defining areas where standard archaeological field techniques (e.g., field walking, shallow geophysical methods, and trial trenching) will be ineffective. Moreover, they may also be useful in determining techniques that have the greatest applicability at the prefieldwork, desk-based planning stage of any project such as establishing areas where the efficacy of aerial photographic analysis will be effective. Thus, the integration of lidar data can provide significant insights into the distribution of archaeological resources and can also provide a vital baseline data set from which to investigate the subsurface. However, in terms of integrating these lidar visualizations within the framework of deposit modelling, other factors must also be considered.

Geoarchaeological deposit models provide a visual representation of the spatial and stratigraphic relationships between subsurface sediments, archaeological features, and palaeoenvironmental remains (Carey et al., 2018). Whilst they vary in their form and presentation, they fundamentally aim to improve the understanding of subsurface sediment architectures and depositional environments that can, in turn, be used to make predictions regarding archaeological potential (Brown et al., 2005; Carey et al., 2017; Chapman et al., 2009;

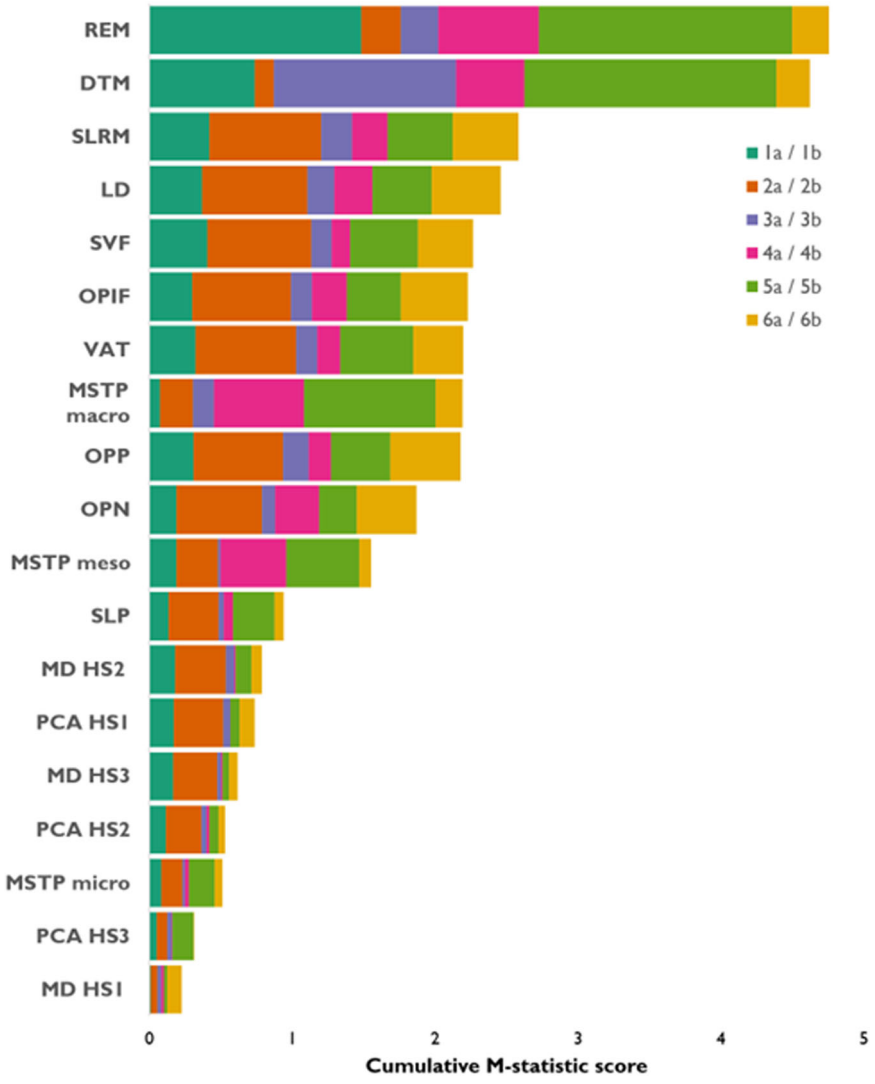

FIGURE 9 Cumulative *M*-statistic scores ranked from best to worst visualization technique.

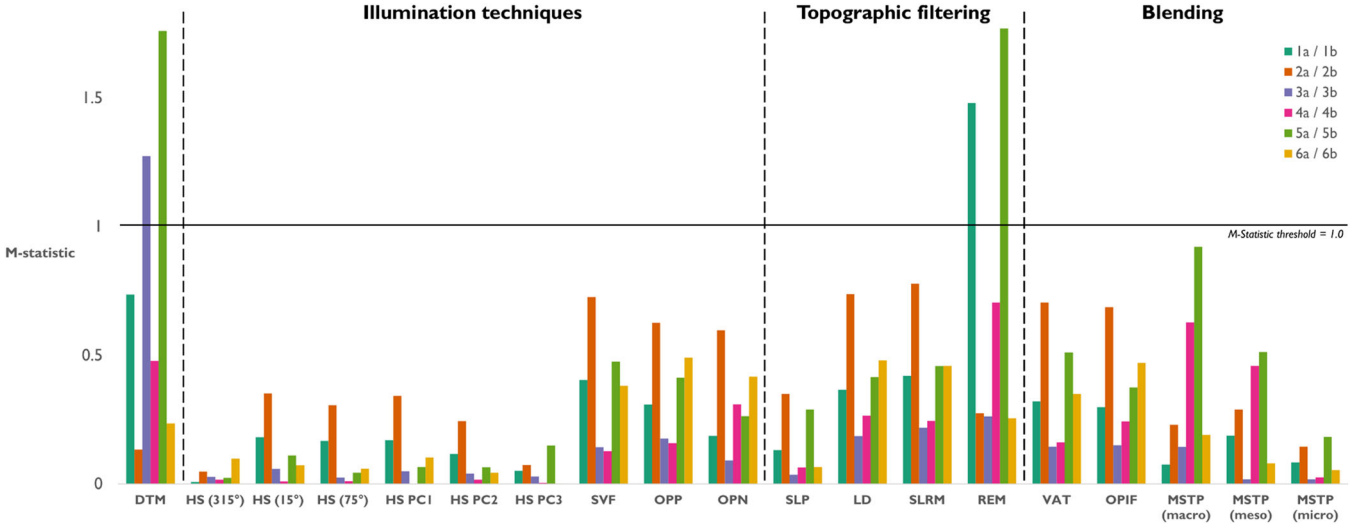

FIGURE 10 Grouped bar chart showing the *M*-statistic calculated for each Regions of Interest (ROI) pair for every visualization technique. Threshold = 1.0, indicated by a solid black line.

TABLE 3 Summary of optimal lidar visualization techniques for the definition of geoarchaeological resources in alluvial environments at different scales.

Landform type	Scale of landform	Optimal visualization method(s)
Palaeochannels, Meander loops, Ridge and swale	Small (5–30 m)	**Simple Local Relief Model (SLRM)**, Local Dominance (LD), Sky-view factor (SVF)
Higher/lower topographic zones, Gravel island, Gravel terrace	Moderate to large (50–250 m+)	**Relative Elevation Model (REM)**, colour-constrained (unaltered) Digital Terrain Model (DTM)

Note: The methods in bold represent those that were the best performing in this analysis; the other techniques listed were also highly effective.

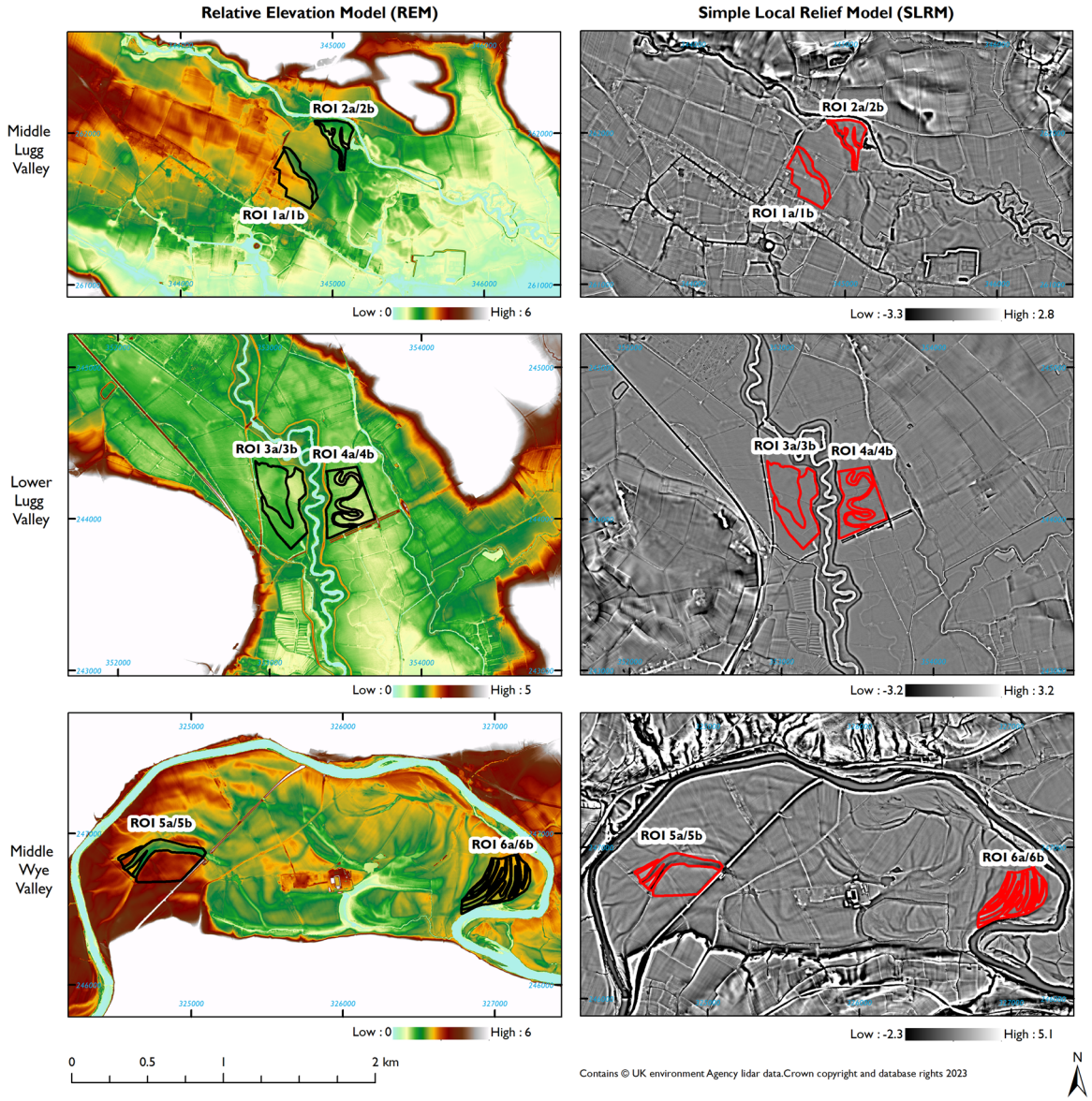

FIGURE 11 Presentation of the most effective lidar visualization techniques together with a simple colour-constrained DTM. DTM, Digital Terrain Models; ROI, Regions of Interest.

Howard et al., 2008). Lidar is somewhat restricted in its capability in this context as it is a 'surface' technique. It does not provide any specific information regarding the subsurface and, therefore, only describes features that are expressed topographically. This is significant as some landforms may not be apparent on the surface due to the deposition of thick alluvial sediments or removal through subsequent erosion and intensive anthropogenic activity (e.g., deep ploughing). Consequently, it is essential that at least some intrusive

works are undertaken (e.g., hand augering, mechanical boreholes, or test-pitting/trial-trenching), which can be further complemented by existing Historic Environment Records (HERs), British Geological Survey (BGS) mapping, other remote sensing data sets (Crabb et al., 2022) and geophysical surveys (Bates & Bates, 2016; Verhegge et al., 2016, 2021).

To facilitate the effective integration of multiple, disparate data sets into deposit models, it can be useful to use consistent projections and datum values. As this can be achieved by simply using unaltered DTM lidar data sets, there is a strong case for incorporating more simplistic visualizations, particularly given that the unaltered DTM achieved very good *M*-statistic separability scores. However, it is possible that landforms can be missed if they are extremely subtle, as significant cross- and down-slope elevation changes may obscure their visualization. Moreover, for these reasons, unaltered DTMs can also be difficult to utilize over wider areas, and other techniques that account for the influence of general topographic trends (e.g., REM and SLRM) may be more reliable, particularly when studying larger alluvial flood plains.

While this study has focused on alluvial environments, it has implications for the application of lidar data where archaeological resources do not lie immediately below the modern ground surface but are buried beneath accumulated sediments (e.g., colluvial, aeolian, coastal, estuarine, and lacustrine deposits). Lidar has been used extensively in geoarchaeological research to study a wide range of different environments (e.g., Bowen et al., 2018; Carlson & Baichtal, 2015; Gregory et al., 2021; Lausanne et al., 2021) and many of these investigations would benefit from the integration of lidar within a deposit modelling framework to define surface evidence for any variations within these complex depositional zones. As such, it would be beneficial to expand this study to evaluate a larger number of landforms and a wider range of environments. However, the results of this research suggest that such an approach provides a robust baseline from which to investigate the subsurface and future research should, therefore, be directed toward ensuring its integration within a more diverse range of settings. However, currently, this is inconsistently implemented, and alternative visualizations beyond the simple display of DEM are rarely considered.

The focused literature search and review provided at the outset of this paper showed that for applications of lidar in geoarchaeological investigations of alluvial environments, approximately half included an interpretation analogous to a deposit model. In each of these cases, lidar data were integrated into the analysis to some extent, but only 18% use visualization techniques to enhance the visibility of resources. Although some visualizations may not always be appropriate or necessary, as this research has shown, they can help to better define a wide range of features and landforms. Moreover, while there has been a barrier in terms of the technological expertise required to produce visualizations, there is now a wide range of open-source toolboxes and plugins available, which improve their accessibility (Hesse, 2013; Kokalj, Zakšek, Oštir, Pehani, et al., 2013; Qiusheng, 2022). Consequently, given the increasingly widespread and open-access nature of data sets, lidar data processed through the suggested methodologies presented here should form part of a standard approach to geoarchaeological deposit modelling, which has landscape evolution at its core.

7 | CONCLUSION

This paper has provided an overview of a range of commonly used lidar image visualization techniques in archaeological and geomorphological research. It highlights their relative advantages and disadvantages within a flood plain setting and provides examples of each of these techniques presented for case studies derived from the River Lugg and Wye Valleys, Herefordshire, UK. Through a quantitative evaluation of their capability, it has been possible to identify a smaller number of the most appropriate methods. This suggests that a combination of REM combined with SLRM offers an optimal approach. However, the original, unaltered DTMs were also very effective and may enable better integration with deposit models as their values are more consistent with other data sets (e.g., intrusive methods, HER records, and geological mapping), especially when depths below ground level are required. However, lidar visualizations can help to better define the distribution of buried deposits of geoarchaeological interest across a site or landscape, which can then be interpreted and further investigated in terms of their archaeological and palaeoenvironmental potential.

As alluvial environments offer the unique challenge of combining rich, well-preserved archaeological and palaeocological records with conditions where archaeological prospection methods are ineffective, appropriate visualization of lidar data has significant potential to aid their investigation. Consequently, it is argued that these techniques should become a standard part of geoarchaeological deposit modelling and future research should aim to apply these methods more widely within river flood plains and other complex depositional zones.

ACKNOWLEDGEMENTS

The authors are also grateful to Dr. Niall Burnside, Richard Higham (University of Brighton), and Robin Jackson (Worcestershire Archaeology) for their assistance with and discussion of aspects of this research. We are also grateful to the two anonymous reviewers for their comments whose comments helped to improve the quality of this paper. This work was supported by the UK's Engineering and Physical Sciences Research Council (EPSRC) grant for the Centre for Doctoral Training: Science and Engineering in Art, Heritage and Archaeology (SEAHA; EP/L016036/1). The open government license lidar data that support the findings of this study are available from the DEFRA Data Services Platform (Department for Environment Food and Rural Affairs, 2021).

ORCID

Nicholas Crabb http://orcid.org/0000-0003-4638-660X
Chris Carey http://orcid.org/0000-0001-7459-9640

REFERENCES

Arnold, N. S., Rees, W. G., Devereux, B. J., & Amable, G. S. (2006). Evaluating the potential of high-resolution airborne LiDAR data in glaciology. *International Journal of Remote Sensing*, *27*, 1233–1251. https://doi.org/10.1080/01431160500353817

Bakuła, K., Salach, A., Zelaya Wziątek, D., Ostrowski, W., Górski, K., & Kurczyński, Z. (2017). Evaluation of the accuracy of lidar data acquired using a UAS for levee monitoring: Preliminary results. *International Journal of Remote Sensing*, *38*, 2921–2937. https://doi.org/10.1080/01431161.2016.1277044

Bates, C. R., & Bates, M. R. (2016). Palaeogeographic reconstruction in the transition zone: The role of geophysical forward modelling in ground investigation surveys. *Archaeological Prospection*, *23*, 311–323. https://doi.org/10.1002/arp.1546

Bennett, R., Cowley, D., & De Laet, V. (2014). The data explosion: Tackling the taboo of automatic feature recognition in airborne survey data. *Antiquity*, *88*, 896–905. https://doi.org/10.1017/S0003598X00050766

Bennett, R., Welham, K., Hill, R., & Ford, A. (2012). A comparison of visualization techniques for models created from airborne laser scanned data. *Archaeological Prospection*, *19*, 41–48. https://doi.org/10.1002/arp.1414

Bini, M., Rossi, V., Amorosi, A., Pappalardo, M., Sarti, G., Noti, V., Capitani, M., Fabiani, F., & Gualandi, M. L. (2015). Palaeoenvironments and palaeotopography of a multilayered city during the Etruscan and Roman periods: Early interaction of fluvial processes and urban growth at Pisa (Tuscany, Italy). *Journal of Archaeological Science*, *59*, 197–210. https://doi.org/10.1016/j.jas.2015.04.005

Bluesky International Ltd. (2022). *LiDAR applications* [White Paper].

Bonhage, A., Eltaher, M., Raab, T., Breuß, M., Raab, A., & Schneider, A. (2021). A modified mask region-based convolutional neural network approach for the automated detection of archaeological sites on high-resolution light detection and ranging-derived digital elevation models in the North German Lowland. *Archaeological Prospection*, *28*, 177–186. https://doi.org/10.1002/arp.1806

Borland, D., & Taylor Ii, R. M. (2007). Rainbow color map (still) considered harmful. *IEEE Computer Graphics and Applications*, *27*, 14–17. https://doi.org/10.1109/MCG.2007.323435

Bowen, M. W., Johnson, W. C., & King, D. A. (2018). Spatial distribution and geomorphology of Lunette dunes on the high plains of Western Kansas: Implications for geoarchaeological and paleoenvironmental research. *Physical Geography*, *39*, 21–37. https://doi.org/10.1080/02723646.2017.1319683

Brolly, M., Simard, M., Tang, H., Dubayah, R. O., & Fisk, J. P. (2016). A Lidar-Radar framework to assess the impact of vertical forest structure on interferometric coherence. *IEEE Journal of Selected Topics in Applied Earth Observations and Remote Sensing*, *9*, 5830–5841. https://doi.org/10.1109/JSTARS.2016.2527360

Brown, A. G. (2009). Colluvial and alluvial response to land use change in Midland England: An integrated geoarchaeological approach. *Geomorphology*, *108*, 92–106. https://doi.org/10.1016/j.geomorph.2007.12.021

Brown, A. G. (1997). Alluvial geoarchaeology; floodplain archaeology and environmental change, alluvial geoarchaeology; floodplain archaeology and environmental change. *Cambridge Manuals in Archaeology*. Cambridge University Press.

Brown, A. G., Carey, C., Challis, K., Howard, A. J., & Cooper, L. (2005). Predictive modelling of multi-period geoarchaeological ressources at river confluence. Archaeology Data Service. https://doi.org/10.5284/1000174

Brunning, R., & Farr-Cox, F. (2005). The River Siger rediscovered: LIDAR survey and relict landscape on the Somerset claylands. In *Archaeology in the Severn Estuary* (Vol. *16*, pp. 7–15). https://doi.org/10.5284/1069527

Bundzel, M., Jaščur, M., Kováč, M., Lieskovský, T., Sinčák, P., & Tkáčik, T. (2020). Semantic segmentation of airborne LiDAR data in Maya archaeology. *Remote Sensing*, *12*, 3685. https://doi.org/10.3390/rs12223685

Campbell, J., & Shin, M. (2011). *Essentials of geographic information systems*. Saylor Foundation.

Carey, C., Howard, A. J., Corcoran, J., Knight, D., & Heathcote, J. (2019). Deposit modeling for archaeological projects: Methods, practice, and future developments. *Geoarchaeology*, *34*, 495–505. https://doi.org/10.1002/gea.21712

Carey, C., Howard, A. J., Jackson, R., & Brown, A. (2017). Using geoarchaeological deposit modelling as a framework for archaeological evaluation and mitigation in alluvial environments. *Journal of Archaeological Science: Reports*, *11*, 658–673. https://doi.org/10.1016/j.jasrep.2017.01.013

Carey, C., Howard, A. J., Knight, D., Corcoran, J., & Heathcote, J. (2018). *Deposit modelling and archaeology*. Short Run Press: Exeter.

Carey, C. J., Brown, T. G., Challis, K. C., Howard, A. J., & Cooper, L. (2006). Predictive modelling of multiperiod geoarchaeological resources at a river confluence: A case study from the Trent-Soar, UK. *Archaeological Prospection*, *13*, 241–250. https://doi.org/10.1002/arp.295

Carlson, R. J., & Baichtal, J. F. (2015). A predictive model for locating early holocene archaeological sites based on raised shell-bearing strata in southeast Alaska, USA. *Geoarchaeology*, *30*, 120–138. https://doi.org/10.1002/gea.21501

Casana, J., Laugier, E. J., Hill, A. C., Reese, K. M., Ferwerda, C., McCoy, M. D., & Ladefoged, T. (2021). Exploring archaeological landscapes using drone-acquired lidar: Case studies from Hawai'i, Colorado, and New Hampshire, USA. *Journal of Archaeological Science: Reports*, *39*, 103133. https://doi.org/10.1016/j.jasrep.2021.103133

Castanet, C., Purdue, L., Testé, M., Garnier, A., Develle-Vincent, A.-L., Mokadem, F., Hatté, C., Gauthier, C., Lanos, P., Dufresne, P., Lemonnier, E., Dussol, L., Hiquet, J., & Nondédéo, P. (2022). Multi-millennial human impacts and climate change during the maya early Anthropocene: Implications on hydro-sedimentary dynamics and socio-environmental trajectories (Naachtun, Guatemala). *Quaternary Science Reviews*, *283*, 107458. https://doi.org/10.1016/j.quascirev.2022.107458

Cerrillo-Cuenca, E. (2017). An approach to the automatic surveying of prehistoric barrows through LiDAR. *Quaternary International*, *435*, 135–145. https://doi.org/10.1016/j.quaint.2015.12.099

Challis, K. (2006). Airborne laser altimetry in alluviated landscapes. *Archaeological Prospection*, *13*, 103–127. https://doi.org/10.1002/arp.272

Challis, K., Carey, C., Kincey, M., & Howard, A. J. (2011). Assessing the preservation potential of temperate, lowland alluvial sediments using airborne Lidar intensity. *Journal of Archaeological Science*, *38*, 301–311. https://doi.org/10.1016/j.jas.2010.09.006

Challis, K., Forlin, P., & Kincey, M. (2011). A generic toolkit for the visualization of archaeological features on airborne LiDAR elevation data. *Archaeological Prospection*, *18*, 279–289. https://doi.org/10.1002/arp.421

Challis, K., & Howard, A. J. (2006). A review of trends within archaeological remote sensing in alluvial environments. *Archaeological Prospection*, *13*, 231–240. https://doi.org/10.1002/arp

Challis, K., & Howard, A. J. (2003). GIS-based modelling of sub-surface deposits for archaeological prospection in alluvial landscapes. In A. Howard, M. Macklin, & D. Passmore (Eds.), *Alluvial Archaeology in Europe: Proceedings of the Alluvial Archaeology of North-West Europe and Mediteranian, 18–19 December 2000, Leeds, UK*.

Challis, K., Kokalj, Z., Kincey, M., Moscrop, D., & Howard, A. J. (2008). Airborne lidar and historic environment records. *Antiquity*, *82*, 1055–1064. https://doi.org/10.1017/S0003598X00097775

Chamberlain, E. L., Mehta, J. M., Reimann, T., & Wallinga, J. (2020). A geoarchaeological perspective on the challenges and trajectories of Mississippi Delta communities. *Geomorphology*, *360*, 107132. https://doi.org/10.1016/j.geomorph.2020.107132

Chapman, H., Adcock, J., & Gater, J. (2009). An approach to mapping buried prehistoric palaeosols of the Atlantic seaboard in Northwest Europe using GPR, geoarchaeology and GIS and the implications for heritage management. *Journal of Archaeological Science*, *36*, 2308–2313. https://doi.org/10.1016/j.jas.2009.06.015

Chiba, T., Kaneta, S., & Suzuki, Y. (2008). Red relief image Map1: New visualization method for three-dimensional data. *The International Archives of Photogrammetry, Remote Sensing and Spatial Information Sciences* (Vol. XXXVII, Part B2).

Coe, D. (2022). *Creating REMs in QGIS with the IDW Method* [WWW Document]. https://dancoecarto.com/creating-rems-in-qgis-the-idw-method

Corrò, E., & Mozzi, P. (2017). Water matters. Geoarchaeology of the city of Adria and palaeohydrographic variations (Po Delta, Northern Italy). *Journal of Archaeological Science: Reports*, *15*, 482–491. https://doi.org/10.1016/j.jasrep.2016.08.001

Crabb, N., Carey, C., Howard, A. J., Jackson, R., Burnside, N., & Brolly, M. (2022). Modelling geoarchaeological resources in temperate alluvial environments: The capability of higher resolution satellite remote sensing techniques. *Journal of Archaeological Science*, *141*, 105576. https://doi.org/10.2139/ssrn.3961261

Crutchley, S., & Crow, P. (2010). *The light fantastic: Using airborne lidar in archaeological survey*. English Heritage.

Danese, M., Gioia, D., Vitale, V., Abate, N., Amodio, A. M., Lasaponara, R., & Masini, N. (2022). Pattern recognition approach and LiDAR for the analysis and mapping of archaeological looting: application to an Etruscan Site. *Remote Sensing*, *14*, 1587. https://doi.org/10.3390/rs14071587

Davis, D. S. (2019). Object-based image analysis: A review of developments and future directions of automated feature detection in landscape archaeology. *Archaeological Prospection*, *26*, 155–163. https://doi.org/10.1002/arp.1730

Davis, O. (2012). *Processing and working with LiDAR data in ArcGIS: A practical guide for archaeologists*. The Royal Commission on the Ancient and Historical Monuments of Wales.

De Reu, J., Bourgeois, J., Bats, M., Zwertvaegher, A., Gelorini, V., De Smedt, P., Chu, W., Antrop, M., De Maeyer, P., Finke, P., Van Meirvenne, M., Verniers, J., & Crombé, P. (2013). Application of the topographic position index to heterogeneous landscapes. *Geomorphology*, *186*, 39–49. https://doi.org/10.1016/j.geomorph.2012.12.015

Department for Environment Food and Rural Affairs. (2021). *Defra Data Services Platform* [WWW Document]. https://environment.data.gov.uk/DefraDataDownload/

Devereux, B. J., Amable, G. S., & Crow, P. (2008). Visualisation of LiDAR terrain models for archaeological feature detection. *Antiquity*, *82*, 470–479. https://doi.org/10.1017/S0003598X00096952

Dilts, T. E., Yang, J., & Weisberg, P. J. (2010). Mapping riparian vegetation with lidar data. *ArcUser*, *4*.

van Dinter, M., Cohen, K. M., Hoek, W. Z., Stouthamer, E., Jansma, E., & Middelkoop, H. (2017). Late Holocene lowland fluvial archives and geoarchaeology: Utrecht's case study of Rhine river abandonment under Roman and Medieval settlement. *Quaternary Science Reviews*, *166*, 227–265. https://doi.org/10.1016/j.quascirev.2016.12.003

Dinn, J., & Roseff, R. (1992). Alluvium and archaeology in the Herefordshire valleys. In S. Needham, & M. Macklin (Eds.), *Alluvial Archaeology in Britain: Proceedings of a Conference Sponsored by the RMC Group Plc 2–5 January 1991*, British Museum. (pp. 141–155). Oxbow Monograph 27.

Doneus, M. (2013). Openness as visualization technique for interpretative mapping of airborne lidar derived digital terrain models. *Remote Sensing*, *5*, 6427–6442. https://doi.org/10.3390/rs5126427

Doneus, M., Briese, C., Fera, M., & Janner, M. (2008). Archaeological prospection of forested areas using full-waveform airborne laser scanning. *Journal of Archaeological Science*, *35*, 882–893. https://doi.org/10.1016/j.jas.2007.06.013

Engel, M., Henselowsky, F., Roth, F., Kadereit, A., Herzog, M., Hecht, S., Lindauer, S., Bubenzer, O., & Schukraft, G. (2022). Fluvial activity of the late-glacial to Holocene "Bergstraßenneckar" in the upper Rhine Graben near Heidelberg, Germany—First results. *E&G Quaternary Science Journal*, *71*, 213–226. https://doi.org/10.5194/egqsj-71-213-2022

Environment Agency. (2021). *National LiDAR Programme* [WWW Document]. https://data.gov.uk/dataset/f0db0249-f17b-4036-9e65-309148c97ce4/national-lidar-programme

Europae Archaeologiae Consilium. (2022). *Use of lidar in heritage: EAC seeks your help!* [WWW Document]. eacsite. https://www.europae-archaeologiae-consilium.org/post/use-of-lidar-in-heritage-eac-seeks-your-help

Evans, I. S. (2012). Geomorphometry and landform mapping: What is a landform? *Geomorphology*, *137*(1), 94–106. https://doi.org/10.1016/j.geomorph.2010.09.029

Fontana, A., Vinci, G., Tasca, G., Mozzi, P., Vacchi, M., Bivi, G., Salvador, S., Rossato, S., Antonioli, F., Asioli, A., Bresolin, M., Di Mario, F., & Hajdas, I. (2017). Lagoonal settlements and relative sea level during Bronze Age in Northern Adriatic: Geoarchaeological evidence and paleogeographic constraints. *Quaternary International*, *439*, 17–36. https://doi.org/10.1016/j.quaint.2016.12.038

Freeland, T., Heung, B., Burley, D. V., Clark, G., & Knudby, A. (2016). Automated feature extraction for prospection and analysis of monumental earthworks from aerial LiDAR in the Kingdom of Tonga. *Journal of Archaeological Science*, *69*, 64–74. https://doi.org/10.1016/j.jas.2016.04.011

French, C. (2003). *Geoarchaeology in action: Studies in soil micromorphology and lanscape evolution*. Routledge. https://doi.org/10.4324/9780203987148

Gearey, B., Chapman, H., & Howard, A. J. (2016). *Down by the River archaeological, palaeoenvironmental and geoarchaeological investigations of the Suffolk River valleys*. Oxbow Books.

Gomez-Heras, M., Ortega-Becerril, J. A., Garrote, J., Fort, R., & Lopez-Gonzalez, L. (2019). Morphometric measurements of bedrock rivers at different spatial scales and applications to geomorphological heritage research. *Progress in Earth and Planetary Science*, *6*, 29. https://doi.org/10.1186/s40645-019-0275-0

Gregory, D. J., Bennike, O., Jensen, J. B., Rasmussen, P., & Al-Hamdani, Z. (2021). Development of predictive geoarchaeological models to locate and assess the preservation potential of submerged prehistoric sites using remote sensing, palaeoenvironmental analysis, and GIS. *Heritage*, *4*, 4678–4699. https://doi.org/10.3390/heritage4040258

Guyot, A., Hubert-Moy, L., & Lorho, T. (2018). Detecting neolithic burial mounds from LiDAR-derived elevation data using a multi-scale approach and machine learning techniques. *Remote Sensing*, *10*, 225. https://doi.org/10.3390/rs10020225

Guyot, A., Lennon, M., & Hubert-Moy, L. (2021). Objective comparison of relief visualization techniques with deep CNN for archaeology. *Journal of Archaeological Science: Reports*, *38*, 103027. https://doi.org/10.1016/j.jasrep.2021.103027

Hemingway, J., & Dinn, J. (1996). The Herefordshire valleys survey: Evaluation of field techniques on valley sites in Herefordshire, 28.

Hesse, R. (2016). Visualisierung hochauflösender Digitaler Geländemodelle mit LiVT. In U. Lieberwirt, & I. Herzog (Eds.), *3D-Anwendungen in Der Archäologie, Berlin Studies of the Ancient World* (Vol. *34*. pp. 109–128).

Hesse, R. (2013). Lidar Visualisation Toolbox (LiVT).

Hesse, R. (2010). LiDAR-derived local relief models—A new tool for archaeological prospection. *Archaeological Prospection*, *17*(2), 67–72. https://doi.org/10.1002/arp.374

Historic England. (2018). Using airborne Lidar in archaeological survey: The light fantastic. Historic England.

Historic England. (2020). Deposit modelling and archaeology guidance for mapping buried deposits. Historic England.

Höfle, B., & Rutzinger, M. (2011). Topographic airborne LiDAR in geomorphology: A technological perspective. *Zeitschrift für Geomorphologie, Supplementary Issues*, *55*, 1–29. https://doi.org/10.1127/0372-8854/2011/0055S2-0043

Howard, A. J., Brown, A. G., Carey, C. J., Challis, K., Cooper, L. P., Kincey, M., & Toms, P. (2008). Archaeological resource modelling in temperate river valleys: A case study from the Trent Valley, UK. *Antiquity*, *82*, 1040–1054. https://doi.org/10.1017/S0003598X00097763

Howard, A. J., Kluiving, S. J., Engel, M., & Heyvaert, V. M. A. (2015). Geoarchaeological records in temperate European river valleys: Quantifying the resource, assessing its potential and managing its future. *Quaternary International*, *367*, 42–50. https://doi.org/10.1016/j.quaint.2014.05.003

Howard, A. J., & Macklin, M. G. (1999). A generic geomorphological approach to archaeological interpretation and prospection in British river valleys: A guide for archaeologists investigating Holocene landscapes. *Antiquity*, *73*, 527–541. https://doi.org/10.1017/S0003598X0006508X

Jackson, R., & Miller, D. (2011). *Wellington Quarry, Herefordshire (1986–96): Investigations of a landscape in the Lower Lugg Valley*. Oxbow books.

Jasiewicz, J., & Stepinski, T. F. (2013). Geomorphons—A pattern recognition approach to classification and mapping of landforms. *Geomorphology*, *182*, 147–156. https://doi.org/10.1016/j.geomorph.2012.11.005

Jones, A. F., Brewer, P. A., Johnstone, E., & Macklin, M. G. (2007). High-resolution interpretative geomorphological mapping of river valley environments using airborne LiDAR data. *Earth Surface Processes and Landforms*, *32*, 1574–1592. https://doi.org/10.1002/esp.1505

Jones, H., & Vaughan, R. (2010). *Remote sensing of vegetation: Principles techniques, and applications*. Oxford University Press.

Jones, J. L. (2006). Side channel mapping and fish habitat suitability analysis using lidar topography and orthophotography. *Photogrammetric Engineering and Remote Sensing*, 1202–1206.

Kaufman, Y. J., & Remer, L. A. (1994). Detection of forests using mid-IR reflectance: An application for aerosol studies. *IEEE Transactions on Geoscience and Remote Sensing*, *32*, 672–683. https://doi.org/10.1109/36.297984

Kellner, J. R., Armston, J., Birrer, M., Cushman, K. C., Duncanson, L., Eck, C., Falleger, C., Imbach, B., Král, K., Krůček, M., Trochta, J., Vrška, T., & Zgraggen, C. (2019). New opportunities for forest remote sensing through ultra-high-density drone lidar. *Surveys in Geophysics*, *40*, 959–977. https://doi.org/10.1007/s10712-019-09529-9

Kirk, A. (2019). *Data visualisation: A handbook for data-driven design* (2nd ed.). Sage.

Kokalj, Ž., & Hesse, R. (2017). *Airborne laser scanning raster data visualization: A Guide to Good Practice*. Založba. https://doi.org/10.1073/pnas.1221378110/-/DCSupplemental

Kokalj, Ž., & Oštir, K. (2018). Lidar data visualization and processing. *The Encyclopedia of Archaeological Sciences*, 1–6. https://doi.org/10.1002/9781119188230.saseas0347

Kokalj, Ž., & Somrak, M. (2019). Why not a single image? Combining visualizations to facilitate fieldwork and on-screen mapping. *Remote Sensing*, *11*, 747. https://doi.org/10.3390/rs11070747

Kokalj, Ž., Zakšek, K., & Oštir, K. (2013). Visualizations of lidar derived relief models. In R. Opitz, & D. Cowley (Eds.), *Interpreting Archaeological Topography: 3D Data, Visualisation and Observation* (pp. 100–114). https://doi.org/10.2307/j.ctvh1dqdz.13

Kokalj, Z., Zakšek, K., Oštir, K., Pehani, P., Čotar, K., & Somrak, M. (2019). *RVT manual*, version 2.2.1.

Kokalj, Ž., Zakšek, K., Oštir, K., Pehani, P., Čotar, K., & Somrak, M. (2013). *Relief visualization toolbox (RVT)* [WWW Document]. Research Centre of the Slovenian Academy of Sciences and Arts. https://iaps.zrc-sazu.si/en/rvt#v

van Lanen, R. J., & Pierik, H. J. (2019). Calculating connectivity patterns in delta landscapes: Modelling Roman and early-medieval route networks and their stability in dynamic lowlands. *Quaternary International*, *501*, 393–412. https://doi.org/10.1016/j.quaint.2017.03.009

Lasaponara, R., Coluzzi, R., & Masini, N. (2011). Flights into the past: Full-waveform airborne laser scanning data for archaeological investigation. *Journal of Archaeological Science*, *38*, 2061–2070. https://doi.org/10.1016/j.jas.2010.10.003

Lausanne, A. L., Fedje, D. W., Mackie, Q., & Walker, I. J. (2021). Identifying sites of high geoarchaeological potential using aerial LIDAR and GIS on Quadra Island, Canada. *The Journal of Island and Coastal Archaeology*, *16*, 482–508. https://doi.org/10.1080/15564894.2019.1659884

Lin, S., Chen, N., & He, Z. (2021). Automatic landform recognition from the perspective of watershed spatial structure based on digital elevation models. *Remote Sensing*, *13*, 3926. https://doi.org/10.3390/rs13193926

Lindsay, J. B., Cockburn, J. M. H., & Russell, H. A. J. (2015). An integral image approach to performing multi-scale topographic position analysis. *Geomorphology*, *245*, 51–61. https://doi.org/10.1016/j.geomorph.2015.05.025

Lozić, E., & Štular, B. (2021). Documentation of Archaeology-specific workflow for airborne LiDAR data processing. *Geosciences*, *11*, 26. https://doi.org/10.3390/geosciences11010026

Mayoral, A., Toumazet, J.-P., Simon, F.-X., Vautier, F., & Peiry, J.-L. (2017). The highest gradient model: A new method for analytical assessment of the efficiency of LiDAR-derived visualization techniques for landform detection and mapping. *Remote Sensing*, *9*, 120. https://doi.org/10.3390/rs9020120

Melin, M., Korhonen, L., Kukkonen, M., & Packalen, P. (2017). Assessing the performance of aerial image point cloud and spectral metrics in predicting boreal forest canopy cover. *ISPRS Journal of Photogrammetry and Remote Sensing*, *129*, 77–85. https://doi.org/10.1016/j.isprsjprs.2017.04.018

Melin, M., Shapiro, A. C., & Glover-Kapfer, P. (2017). LIDAR for ecology and conservation. *WWF Conservation Technology Series*, *1*, 40.

van der Meulen, B., Cohen, K. M., Pierik, H. J., Zinsmeister, J. J., & Middelkoop, H. (2020). LiDAR-derived high-resolution palaeo-DEM construction workflow and application to the early medieval lower Rhine valley and upper delta. *Geomorphology*, *370*, 107370. https://doi.org/10.1016/j.geomorph.2020.107370

Meyer, M., Pfeffer, I., & Jürgens, C. (2019). Automated detection of field monuments in digital terrain models of Westphalia using OBIA. *Geosciences*, *9*, 109. https://doi.org/10.3390/geosciences9030109

Mozzi, P., Ferrarese, F., Zangrando, D., Gamba, M., Vigoni, A., Sainati, C., Fontana, A., Ninfo, A., Piovan, S., Rossato, S., & Veronese, F. (2018). The modeling of archaeological and geomorphic surfaces in a multistratified urban site in Padua, Italy. *Geoarchaeology*, *33*, 67–84. https://doi.org/10.1002/gea.21641

Niculiță, M. (2020). Geomorphometric methods for burial mound recognition and extraction from high-resolution LiDAR DEMs. *Sensors*, *20*, 1192. https://doi.org/10.3390/s20041192

Ninfo, A., Fontana, A., Mozzi, P., & Ferrarese, F. (2011). Remote sensing and LiDAR applications in the alluvial geoarchaeology of NE Italy. *Alpine and Mediterranean Quaternary*, *24*, 194–196.

Ninfo, A., Mozzi, P., & Abbà, T. (2016). Integration of LiDAR and cropmark remote sensing for the study of fluvial and anthropogenic landforms in the Brenta-Bacchiglione alluvial plain (NE Italy). *Geomorphology*, *260*, 64–78. https://doi.org/10.1016/j.geomorph.2015.11.006

Notebaert, B., Verstraeten, G., Govers, G., & Poesen, J. (2009). Qualitative and quantitative applications of LiDAR imagery in fluvial geomorphology. *Earth Surface Processes and Landforms*, *34*, 217–231. https://doi.org/10.1002/esp.1705

Olson, P., Legg, N., Abbe, T., Reinhart, M., & Radloff, J. (2014). *A methodology for delineating planning-level channel migration zones (No. 14- 06–025)*. Department of Ecology: State of Washington.

Opitz, R. S., & Cowley, D. C. (2013). *Interpreting archaeological topography: Airborne Laser Scanninf, 3D data and ground observation, Interpreting Archaeological Topography*. Oxbow books. https://doi.org/10.2307/j.ctvh1dqdz.6

Orengo, H. A., & Petrie, C. A. (2018). Multi-scale relief model (MSRM): A new algorithm for the visualization of subtle topographic change of variable size in digital elevation models: MSRM: An algorithm for the multi-scale analysis of topographic change. *Earth Surface Processes and Landforms*, *43*, 1361–1369. https://doi.org/10.1002/esp.4317

Pádua, L., Vanko, J., Hruška, J., Adão, T., Sousa, J. J., Peres, E., & Morais, R. (2017). UAS, sensors, and data processing in agroforestry: A review towards practical applications. *International Journal of Remote Sensing*, *38*, 2349–2391. https://doi.org/10.1080/01431161.2017.1297548

Passmore, D. G., & Waddington, C. (2009). *Managing archaeological landscapes in Northumberland: Till tweed studies* (Vol. 1). Oxbow Books.

Pears, B., Brown, A. G., Carroll, J., Toms, P., Wood, J., & Jones, R. (2020). Early medieval place-names and riverine flood histories: A new approach and new chronostratigraphic records for three English rivers. *European Journal of Archaeology*, *23*, 381–405. https://doi.org/10.1017/eaa.2019.72

Qiusheng, W. (2022). *WhiteBox tools: ArcGIS plugin* [WWW Document]. https://www.whiteboxgeo.com/manual/wbt_book/arcgis_plugin.html

rapidlasso GmbH. (2021). *LAStools* [WWW Document]. https://rapidlasso.com/lastools/

Resop, J. P., Lehmann, L., & Hession, W. C. (2019). Drone laser scanning for modeling riverscape topography and vegetation: Comparison with traditional aerial lidar. *Drones*, *3*, 35. https://doi.org/10.3390/drones3020035

Richards, J. (2013). *Remote sensing digital image analysis: An introduction* (5th ed.). Springer.

Risbøl, O., & Gustavsen, L. (2018). LiDAR from drones employed for mapping archaeology—Potential, benefits and challenges. *Archaeological Prospection*, *25*, 329–338. https://doi.org/10.1002/arp.1712

Schmidt, J., Rabiger-Völlmer, J., Werther, L., Werban, U., Dietrich, P., Berg, S., Ettel, P., Linzen, S., Stele, A., Schneider, B., & Zielhofer, C. (2019). 3D-Modelling of Charlemagne's summit canal (Southern Germany)—Merging remote sensing and geoarchaeological subsurface data. *Remote Sensing*, *11*, 1111. https://doi.org/10.3390/rs11091111

Schneider, A., Takla, M., Nicolay, A., Raab, A., & Raab, T. (2015). A template-matching approach combining morphometric variables for automated mapping of charcoal kiln sites. *Archaeological Prospection*, *22*, 45–62. https://doi.org/10.1002/arp.1497

Sevara, C., Pregesbauer, M., Doneus, M., Verhoeven, G., & Trinks, I. (2016). Pixel versus object—A comparison of strategies for the semi-automated mapping of archaeological features using airborne laser scanning data. *Journal of Archaeological Science: Reports*, *5*, 485–498. https://doi.org/10.1016/j.jasrep.2015.12.023

Smith, M. J., & Clark, C. D. (2005). Methods for the visualization of digital elevation models for landform mapping. *Earth Surface Processes and Landforms*, *30*, 885–900. https://doi.org/10.1002/esp.1210

Stastney, P., Scaife, R., Carretero, L. G., Whittaker, J. E., Cameron, N., & Allison, E. (2021). Modelling prehistoric topography and vegetation in the lower thames valley, UK: Palaeoenvironmental context for Wetland Archaeology and evidence for Neolithic Landnám from North Woolwich. *Environmental Archaeology*, *26*, 1–17. https://doi.org/10.1080/14614103.2021.1880683

Stein, S., Malone, S., Knight, D., J. Howard, A., & Carey, C. (2017). New approaches to mapping and managing palaeochannel resources in the light of future environmental change: A case study from the Trent Valley, UK. *The Historic Environment: Policy & Practice*, *8*, 113–124. https://doi.org/10.1080/17567505.2017.1317086

Stott, D., Boyd, D., Beck, A., & Cohn, A. (2015). Airborne LiDAR for the detection of archaeological vegetation marks using biomass as a proxy. *Remote Sensing*, *7*, 1594–1618. https://doi.org/10.3390/rs70201594

Štular, B., Eichert, S., & Lozić, E. (2021). Airborne LiDAR point cloud processing for archaeology. Pipeline and QGIS toolbox. *Remote Sensing*, *13*, 3225. https://doi.org/10.3390/rs13163225

Štular, B., Kokalj, Ž., Oštir, K., & Nuninger, L. (2012). Visualization of lidar-derived relief models for detection of archaeological features. *Journal of Archaeological Science*, *39*, 3354–3360. https://doi.org/10.1016/j.jas.2012.05.029

Štular, B., Lozić, E., & Eichert, S. (2021). Airborne LiDAR-derived digital elevation model for archaeology. *Remote Sensing*, *13*, 1855. https://doi.org/10.3390/rs13091855

Swain, P. H., & Davis, S. M. (1978). *Remote sensing: The quantative approach*. McGraw-Hill.

Szypuła, B. (2017). *Digital elevation models in geomorphology, hydro-geomorphology—Models and trends*. IntechOpen. https://doi.org/10.5772/intechopen.68447

Telling, J., Lyda, A., Hartzell, P., & Glennie, C. (2017). Review of Earth science research using terrestrial laser scanning. *Earth-Science Reviews*, *169*, 35–68. https://doi.org/10.1016/j.earscirev.2017.04.007

Thompson, A. E. (2020). Detecting classic maya settlements with Lidar-derived relief visualizations. *Remote Sensing*, *12*, 2838. https://doi.org/10.3390/rs12172838

Trier, Ø. D., Cowley, D. C., & Waldeland, A. U. (2019). Using deep neural networks on airborne laser scanning data: Results from a case study of semi-automatic mapping of archaeological topography on Arran, Scotland. *Archaeological Prospection*, *26*, 165–175. https://doi.org/10.1002/arp.1731

Trier, Ø. D., & Pilø, L. H. (2012). Automatic detection of pit structures in airborne laser scanning data. *Archaeological Prospection*, *19*, 103–121. https://doi.org/10.1002/arp.1421

Trier, Ø. D., Reksten, J. H., & Løseth, K. (2021). Automated mapping of cultural heritage in Norway from airborne lidar data using faster R-CNN. *International Journal of Applied Earth Observation and Geoinformation*, *95*, 102241. https://doi.org/10.1016/j.jag.2020.102241

Tso, B., & Mather, P. (2009). *Classification methods for remotely sensed data, paper knowledge*. CRC Press. https://doi.org/10.1201/9781420090741

van Valkenburgh, P., Cushman, K. C., Butters, L. J. C., Vega, C. R., Roberts, C. B., Kepler, C., & Kellner, J. (2020). Lasers without lost cities: using drone lidar to capture architectural complexity at Kuelap, Amazonas, Peru. *Journal of Field Archaeology*, *45*, S75–S88. https://doi.org/10.1080/00934690.2020.1713287

Verhegge, J., Missiaen, T., & Crombé, P. (2016). Exploring integrated geophysics and geotechnics as a paleolandscape reconstruction tool: Archaeological prospection of (Prehistoric) sites buried deeply below the Scheldt polders (NW Belgium): geophysics and geotechnics as a palaeolandscape reconstruction tool. *Archaeological Prospection*, *23*, 125–145. https://doi.org/10.1002/arp.1533

Verhegge, J., Storme, A., Cruz, F., & Crombé, P. (2021). Cone penetration testing for extensive mapping of deeply buried Late Glacial cover-sand landscape paleotopography. *Geoarchaeology*, *36*, 130–148. https://doi.org/10.1002/gea.21815

Verschoof-van der Vaart, W. B., & Lambers, K. (2022). Applying automated object detection in archaeological practice: A case study from the southern Netherlands. *Archaeological Prospection*, *29*, 15–31. https://doi.org/10.1002/arp.1833

Verschoof-van der Vaart, W. B., & Lambers, K. (2019). Learning to look at LiDAR: The use of R-CNN in the automated detection of archaeological objects in LiDAR data from the Netherlands. *Journal of Computer Applications in Archaeology*, *2*, 31–40. https://doi.org/10.5334/jcaa.32

Verschoof-van der Vaart, W. B., Lambers, K., Kowalczyk, W., & Bourgeois, Q. P. J. (2020). Combining deep learning and location-based ranking for large-scale archaeological prospection of LiDAR data from the Netherlands. *ISPRS International Journal of Geo-Information*, *9*, 293. https://doi.org/10.3390/ijgi9050293

Wang, D., Laffan, S. W., Liu, Y., & Wu, L. (2010). Morphometric characterisation of landform from DEMs. *International Journal of Geographical Information Science*, *24*, 305–326. https://doi.org/10.1080/13658810802467969

White, D. (2013). LIDAR, point clouds, and their archaeological applications. In D. Comer, & M. Harrower (Eds.), *Mapping archaeological landscapes from space* (pp. 175–186). Springer.

Yokoyama, R., Shlrasawa, M., & Pike, R. J. (2002). *Visualizing topography by openness: A new application of image processing to digital elevation models: Photogrammetric Engineering & Remote Sensing*, *68*(3), 257–265.

Zakšek, K., Oštir, K., & Kokalj, Ž. (2011). Sky-view factor as a relief visualization technique. *Remote Sensing*, *3*, 398–415. https://doi.org/10.3390/rs3020398

SUPPORTING INFORMATION

Additional supporting information can be found online in the Supporting Information section at the end of this article.

How to cite this article: Crabb, N., Carey, C., Howard, A. J., & Brolly, M. (2023). Lidar visualization techniques for the construction of geoarchaeological deposit models: An overview and evaluation in alluvial environments. *Geoarcheology*, 1–25. https://doi.org/10.1002/gea.21959